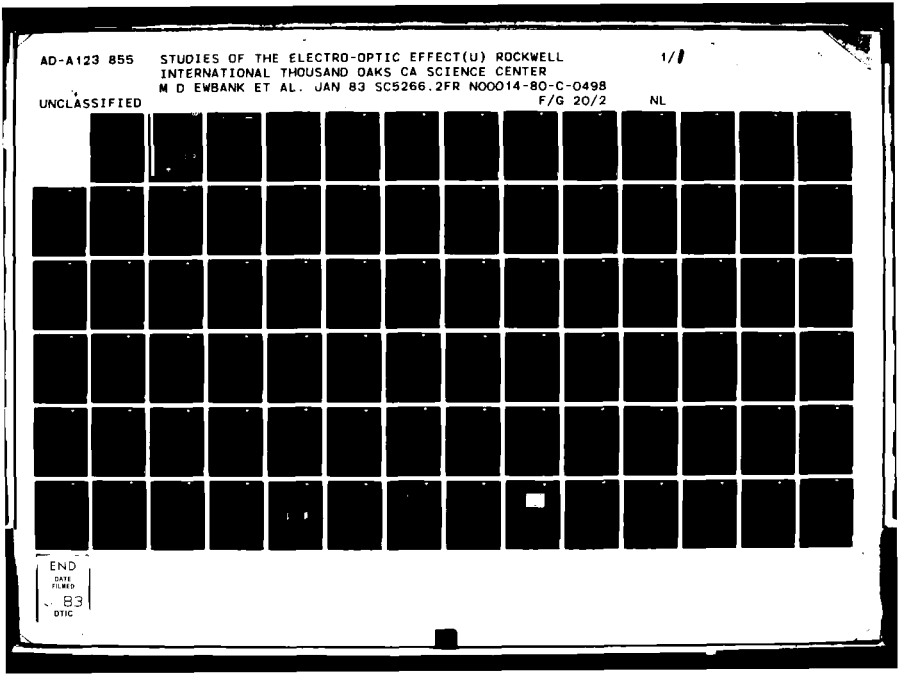
AD-A123 855
STUDIES OF THE ELECTRO-OPTIC EFFECT(U) ROCKWELL INTERNATIONAL THOUSAND OAKS CA SCIENCE CENTER
M D EWBANK ET AL. JAN 83 SC5266.2FR N00014-80-C-0498
1/1
UNCLASSIFIED
F/G 20/2
NL
END
DATE FILMED
83
DTIC

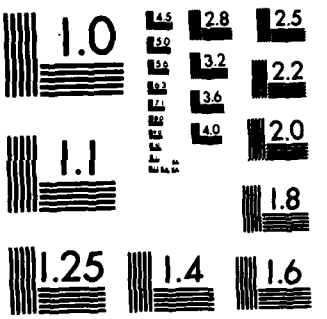

SC5266.2FR

Copy No. 9

STUDIES OF THE ELECTRO-OPTIC EFFECT

FINAL REPORT (PHASE II) FOR THE PERIOD June 1, 1981 through September 30, 1982

CONTRACT NO. N00014-80-C-0498

Prepared for

Office of Naval Research
800 North Quincy Street
Arlington, VA 22217

M.D. Ewbank
P.R. Newman
Principal Investigators

JANUARY 1983

Approved for public release; distribution unlimited

Rockwell International
Science Center

UNCLASSIFIED

SECURITY CLASSIFICATION OF THIS PAGE (When Data Entered)

REPORT DOCUMENTATION PAGE	READ INSTRUCTIONS BEFORE COMPLETING FORM
1. REPORT NUMBER	2. GOVT ACCESSION NO. A123855 / 3. RECIPIENT'S CATALOG NUMBER
4. TITLE (and Subtitle) STUDIES OF THE ELECTRO-OPTIC EFFECT	5. TYPE OF REPORT & PERIOD COVERED Final Report (Phase II) for period 06/01/81 - 09/30/82
	6. PERFORMING ORG. REPORT NUMBER SC5266.2FR
7. AUTHOR(s) M.D. Ewbank, P.R. Newman	8. CONTRACT OR GRANT NUMBER(s) N00014-80-C-0498
9. PERFORMING ORGANIZATION NAME AND ADDRESS Rockwell International Science Center 1049 Camino Dos Rios Thousand Oaks, California 91360	10. PROGRAM ELEMENT, PROJECT, TASK AREA & WORK UNIT NUMBERS NR 372-909 (427)
11. CONTROLLING OFFICE NAME AND ADDRESS Office of Naval Research 800 North Quincy Street Arlington, VA 22217	12. REPORT DATE January 1983
	13. NUMBER OF PAGES 80
14. MONITORING AGENCY NAME & ADDRESS(if different from Controlling Office)	15. SECURITY CLASS. (of this report) Unclassified
	15a. DECLASSIFICATION/DOWNGRADING SCHEDULE

16. DISTRIBUTION STATEMENT (of this Report)

Approved for public release; distribution unlimited.

17. DISTRIBUTION STATEMENT (of the abstract entered in Block 20, if different from Report)

18. SUPPLEMENTARY NOTES

19. KEY WORDS (Continue on reverse side if necessary and identify by block number)

Electro-optics, nonlinear optics, optical materials, predictive methodology, band orbital model, tight-binding theory, dielectric susceptibilities, lattice dynamics, transverse effective charge, tellurium dioxide, thallium arsenic selenide.

20. ABSTRACT (Continue on reverse side if necessary and identify by block number)

A microscopic understanding of the electro-optic effect in crystalline solids has been pursued by employing a tight-binding theory for dielectric susceptibilities. The electronic and lattice contributions to the second-order electro-optic susceptibility have been treated separately and the lattice response of a crystal to an external dc electric field has been investigated in a general formalism. The theory has been specifically applied to the compound, tellurium dioxide. In addition, an experimental determination of the electro-optic coefficient, r_e, in thallium arsenic selenide

DD FORM 1 JAN 73 1473 EDITION OF 1 NOV 65 IS OBSOLETE

UNCLASSIFIED

SECURITY CLASSIFICATION OF THIS PAGE (When Data Entered)

has been made.

TABLE OF CONTENTS

LIST OF FIGURES

FOREWORD

This report to the Office of Naval Research is the concluding final report for a two-year theoretical and experimental effort carried out under Contract N00014-80-C-0498, and covers the period May 13, 1981 to September 31, 1982. The program was carried out at the Rockwell International Science Center and was managed by Dr. Paul R. Newman. The Principal Investigators were Mr. Mark D. Ewbank and Dr. Newman. Prof. Walter A. Harrison of Stanford University was a consultant on the theoretical aspects of this program. Valuable contributions were also made by Prof. Eitan Ehrenfreund of the Technion Institute of Israel, and Dr. Pochi Yeh, Mr. Randolph L. Hall and Dr. M. Khoshnevisan of the Science Center. The Contract Monitor for the Office of Naval Research was Dr. George Wright.

1.0 INTRODUCTION

1.1 Program Objectives

The long-range goal of this program was to theoretically investigate the microscopic physical origins of the linear dc electro-optic effect. A secondary objective was to use the formalism resulting from that investigation to develop a general methodology with predictive capabilities that requires only atomic structure and elemental composition as input.

Additionally, as new increasingly high-performance materials are required by electro-optic device technology, an experimental effort was carried out, not only to provide feedback for the theoretical studies, but to provide data on new and potentially interesting Pockel's electro-optic materials.

1.2 Previous Work

The previous year's work was first devoted to separating the physical sources of the electro-optic effect into those which result primarily from electronic effects, and those associated with lattice dynamics or "ionic-displacive" effects. The Bond Orbital Model[1] was then modified so that the electronic contribution to the electro-optic effect could be calculated simply and straightforwardly using "universal atomic" parameters and numerical sums over chemical bonds in the crystallographic unit cell. This theory was then tested against TeO_2 and predicted an identically zero electronic contribution to the electro-optic tensor in agreement with Kleinman's[2] symmetry relations.

The effort next focussed on the ionic displacive part. Here a further distinction was made between relative motions between ions which do not result in a change in the unit cell dimensions and those which do. The approach, which had not been completely evolved at the conclusion of the first year's effort was to seek a mechanism to calculate the microscopic atomic "spring constants" and relate these to measurable bulk properties such as the Reststrahl frequency or elastic constants.

Finally, the experimental portion of the program was directed towards two compounds: TeO_2 and Tl_3AsSe_3. Measurement on TeO_2 yielded the original characterization[3] of the linear electro-optic effect in terms of the single non-zero component r_{41}. Preliminary measurements of the electro-optic effect in Tl_3AsSe_3 experienced experimental difficulties associated with the semiconducting nature of the material.

1.3 Accomplishments

Significant original results towards understanding the electro-optic effect have been made during this period. The theoretical work, utilizing tight-binding theory and Harrison's "universal atomic parameters"[1] has successfully yielded a formalism for quantitatively calculating both the electronic and ionic contributions to the electro-optic second-order susceptibility. This formalism predicts the electro-optic tensor coefficients utilizing atomic matrix elements, and term values, together with crystallographic coordination and elemental composition, but without any adjustable parameters. As was indicated above, the electronic contribution is calculated in a straightforward manner using tight-binding formalism and bond sums taken over the crystallographic unit cell. Calculations of the contributions due to lattice dynamics has also been successfully reduced to practice and applied to TeO_2. The formalism involves modelling interatomic forces (springs) in terms of a bond-stretching force and a bond-bending force. These interactomic forces can then be used to calculate normal acoustic and optical lattice phonon modes. The calculated frequencies, at zone-center, can then be compared with data derived from optical measurements.

Experimental measurements of the r_c electro-optic tensor component of Tl_3AsSe_3 (TAS) have also been completed. The measurement was complicated by the semiconducting nature of TAS. When several kilovolts were applied to the sample, appreciable current was observed. This resulted in joule heating of the sample and a distortion of the physical dimensions of the crystal as well as concurrent strain-optic effects. This problem was eliminated by using high

voltage pulses instead of a dc voltage and yielded the "unclamped"[4] value for r_c.

1.4 Technical Issues

Although we have demonstrated the utility of our approach to calculations of the electro-optic effect in a specific case, TeO_2, the generality of the method remains untested. Further work on a variety of crystal structures and elemental composition needs to be carried out.

1.5 Report Summary

The remainder of this report is concerned with the technical details for both the theoretical and experimental aspects of this program. The material contained within will provide the basis of at least three future publications, which are currently being completed. Finally, a brief summary of the technical progress, along with some projections for a continuation of work in this general area, will be provided.

2.0 TECHNICAL APPROACH

2.1 Theoretical

First, the connection between the experimental electro-optic coefficients and the theoretical second-order susceptibility tensor is developed. Then a detailed formulation for the dielectric susceptibilities is made in terms of tight-binding theory. Initially, the linear susceptibility is treated and subsequently the model is extended to higher-order susceptibilities. In particular, the electro-optic susceptibility is examined and a technique for evaluating the lattice contribution is presented. Finally, a specific application of the theory is carried out on tellurium dioxide.

2.1.1 Second-Order Susceptibilities and Electro-Optic Coefficients

Experimentally, the determination of the change in refractive index of a crystal due to an applied dc electric field provides a mechanism of measurement of the electro-optic effect. The electro-optic coefficient, r_{ijk}, is defined by the relation[4-6]

$$\Delta(B)_{ij} = \sum_k r_{ijk} E_k \qquad (1)$$

where ΔB_{ij} is the change in the relative optical dielectric impermeability and E_k is the applied electric field. The impermeability is related to the inverse dielectric tensor, ϵ^{-1}, and the refractive index, n, by the expression

$$B_{ij} = (\epsilon^{-1})_{ij} = (n^{-2})_{ij} \quad . \qquad (2)$$

A change in impermeability can be expressed in terms of an index change as

$$\Delta B = -2\Delta n/n^3 \qquad (3)$$

and explicit relationships between Δn and ΔB_{ij} have been derived for optically isotropic, uniaxial and biaxial crystals with the light propagating in an arbitrary direction.[6]

The principal dielectric constant or refractive index can in turn be related to the susceptibility, χ, as

$$n = \sqrt{\varepsilon} = \sqrt{1 + 4\pi\chi} \tag{4}$$

in CGS units. To define higher-order susceptibilities, the induced polarization, P_i, is expanded in terms of increasing powers of electric field[1] as

$$P_i = \sum_j \chi_{ij}^{(1)} E_j + \sum_{jk} \chi_{ijk}^{(2)} E_j E_k + \sum_{jkl} \chi_{ijkl}^{(3)} E_j E_k E_l + \cdots \tag{5}$$

where $\chi_{ij}^{(1)}$ is the linear or first-order susceptibility, $\chi_{ijk}^{(2)}$ is the second-order susceptibility, etc. This form does, however, neglect any frequency dependence. More specifically, the induced, second-order polarization at any given frequency is a function of all three wave-mixing combinations which contribute to that frequency, i.e., integrate the product of the second-order susceptibility with two electric fields over frequency.[7] By considering three special cases in the frequency domain, three distinct second-order susceptibilities have been defined:[8]

$$P_i(2\omega) = \sum_{jk} \chi_{ijk}^{(2)} (2\omega) E_j(\omega) E_k(\omega) \tag{6}$$

$$P_i(\omega = 0) = \sum_{jk} \chi_{ijk}^{(2)} (0) E_j(\omega) E_k(\omega) \tag{7}$$

$$P_i(\omega) = \sum_{jk} \chi^{(2)}_{ikj}(\omega)\, E_j(\omega)\, E_k(0) \qquad (8)$$

which correspond to second harmonic generation, optical rectification and the linear electro-optic effect, respectively. The electro-optic, second-order susceptibility, as defined in Eq. (8), must be symmetric in he indices i and j in order that the total optical susceptibility tensor, $\chi^{(1)}_{ij} + \sum_k \chi^{(2)}_{ikj} E_k$ remain symmetric. This contrasts with the second harmonic generation and optical rectification susceptibilities which are symmetric in all three indices (i, j and k). Keeping these symmetry relations straight is important when dealing with "condensed" notation[5] for the indices because the condensing always occurs on the two symmetric indices. We shall be concentrating on the electro-optic second-order susceptibility, which can be directly related to the electro-optic coefficient,[7,9,10] in CGS units, by

$$r_{ijk} = 4\pi\chi^{(2)}_{ikj}/\epsilon_{ii}/\epsilon_{jj} \qquad (9)$$

where $\epsilon_{ii} = n_i^2 = 1 + 4\pi\chi^{(1)}_{ii}$ is an optical dielectric constant. Note that both r_{ijk} and $\chi^{(2)}_{ikj}(\omega)$ are symmetric in indices i and j which correspond to the dielectric constants appearing in Eq. (9). The theory developed below derives expressions for $\chi^{(2)}_{ikj}(\omega)$ and therefore Eq. (9) will serve as the connection to experiment.

2.1.2 Tight-Binding Calculations of the First-Order Susceptibility

For nominal optical electric fields, the linear susceptibility is usually related to the interband absorptions. These absorptions contribute to an imaginary component of the susceptibility which corresponds to a polarization density that is out of phase with the driving electric field. This absorptive component can be written as

$$\text{Im}\,[\chi_{ij}^{(1)}] = \frac{\pi}{\Omega} \sum_{v,c,\vec{k}\vec{k}'} \langle\psi_c(\vec{k}')|\left(\frac{eh}{m\omega}\right)\frac{\partial}{\partial x_i}|\psi_v(\vec{k})\rangle\langle\psi_v(\vec{k})|\left(\frac{eh}{m\omega}\right)\frac{\partial}{\partial x_j}|\psi_c(\vec{k}')\rangle$$

$$\times\, \delta(E_c(\vec{k}') - E_v(\vec{k}) - h\omega) \qquad (10)$$

where e is the electronic charge, m is the mass of electron and h is Planck's constant divided by 2π. The dipole matrix element is represented by the gradient operator, $\vec{\nabla}$, coupling the occupied (valence) wave function, $|\psi_v(\vec{k})\rangle$, with the unoccupied (conduction) wave function, $|\psi_c(\vec{k}')\rangle$. The delta-function gives a contribution only when the photon energy ($h\omega$) equals the energy difference between the coupled states. Finally, the summation is over wave-vectors of all valence and conduction states in a volume, Ω.

The real part of the linear susceptibility is related to the imaginary component via the Kramers-Kronig relations.[1] By assuming that the dipole matrix elements are independent of frequency, the real part of $\chi^{(1)}$ can be written as

$$\chi_{ij}^{(1)} = \frac{4e^2h^4}{m^2\Omega} \sum_{v,c,\vec{k}} \frac{\langle\psi_c(\vec{k})|\frac{\partial}{\partial x_i}|\psi_v(\vec{k})\rangle\langle\psi_v(\vec{k})|\frac{\partial}{\partial x_j}|\psi_c(\vec{k})\rangle}{(E_c(\vec{k}) - E_v(\vec{k}))^3} \qquad (11)$$

in the limit that the photon frequency is much less than the energy difference between coupled states or zero-frequency limit, (i.e., $h\omega$ is much less than the lowest absorption energy but still greater than the Reststrahl vibrational energies). An extra factor of two has been included in Eq. (11) to account for the two spins associated with each state and the summation over wave-vector, $\vec{k}'$, has been omitted by considering only "vertical transitions." Also, note that the designation of the real part is not explicitly shown in

Eq. (11) since only the real components of the susceptibilities will be considered in the rest of the formalism that follows.

2.1.2.1 Tight-Binding Theory

In the context of tight-binding theory, the dipole matrix elements in Eq. (11) can be expanded in terms of localized Wannier functions, which in turn are written as a summation of Bloch functions. Specifically, the valence-band state, $\psi_v(\vec{k})$, can be expressed as

$$|\psi_v(\vec{k})\rangle = \frac{1}{\sqrt{N}} \sum_m |a_v(\vec{R}_m)\rangle e^{i\vec{k}\cdot\vec{R}_m} \tag{12}$$

where $a_v(\vec{R}_m)$ is the valence Wannier function located at site, $\vec{R}_m$, in the m-th primitive cell and the summation is over N primitive cells. The conduction-band wave function is represented in an analogous fashion. By carrying out this expansion of the dipole matrix elements in Wannier functions, the double summation over sites in each of N primitive cells reduces to N times a single summation. This is because for any particular dipole matrix element involving two Wannier functions there are only N identical matrix elements of Wannier functions on nearest neighbor sites which are non-negligible. Then, the summation over N primitive cells becomes a summation over nearest neighbors. Finally, the dipole matrix element in Eq. (11) is written in terms of Wannier functions as

$$\langle\psi_c(\vec{k})|\frac{\partial}{\partial x_i}|\psi_v(\vec{k})\rangle = \sum_m^{(nn)} \langle a_c(\vec{R}_1)|\frac{\partial}{\partial x_i}|a_v(\vec{R}_m)\rangle e^{i\vec{k}\cdot(\vec{R}_m-\vec{R}_1)} \tag{13}$$

where $\vec{R}_1$ specifies a "central" primitive cell conduction-state site and the summation is over only those valence-state sites $\vec{R}_m$ which are nearest neighbors (nn) to this conduction-state site $\vec{R}_1$ (including the valence states on the same site).

Furthermore, when this dipole matrix element is substituted back into the expression for the linear susceptibility, it is recognized that the wave-vector dependence of the energy difference denominator is negligible (since the energy variation with $\vec{k}$ is small compared to the energy separation between valence and conduction states). Also, the summation over wave-vector can be eliminated because the sinusoidal factor integrated over $\vec{k}$ contributes only at a single, localized valence-state site. Then the linear susceptibility can be expressed as

$$\chi_{ij}^{(1)} = \frac{4e^2\hbar^4}{m^2\Omega} \sum_{v,c,m}^{(nn)} \frac{\langle a_c(\vec{R}_1)|\frac{\partial}{\partial x_i}|a_v(\vec{R}_m)\rangle\langle a_v(\vec{R}_m)|\frac{\partial}{\partial x_j}|a_c(\vec{R}_1)\rangle}{(E_c - E_v)^3} \qquad (14)$$

where the summation includes only those nearest neighbor valence and conduction Wannier functions, located at sites $\vec{R}_m$ and $\vec{R}_1$, respectively.

Typically, the Wannier functions have been chosen by incorporating nature of the chemical bonding of the particular crystal under consideration. For example, the tetrahedral semiconductors have four bond orbitals per primitive cell from which four valence-band Wannier functions are derived from the four antibond orbitals. By focusing on only those dipole matrix elements of the gradient between bonding orbitals, $|b\rangle$, and antibonding orbitals, $|a\rangle$, in the same bond, the summations over nearest neighbor valence and conduction states became a summation over bonds. For ionic compounds, such as the alkali halides, the valence- and conduction-band Wannier functions are adequately represented by the halide-p and alkali-s atomic orbitals, respectively. In this case, the summation over band states became a summation of spσ couplings over the six nearest neighbors.

However, it is not necessary to specify the chemical bonding of the crystal at this point in the formalism. Nothing is lost in generality by representing the Wannier functions by a complete set of valence-electron atomic orbitals: $|s\rangle$, $|p_x\rangle$, $|p_y\rangle$, $|p_z\rangle$, etc. For example, in the above case

of the tetrahedral semiconductors, hybrid sp_3 bonding and antibonding orbitals (and corresponding matrix elements) are simply derived from the appropriate linear combinations of atomic orbitals. Then, from Eq. (14), the dipole matrix elements are between atomic orbitals and the summation over nearest neighbor valence and conduction Wannier functions becomes a sum over all nearest neighbor pairs of atomic orbitals in the primitive cell.

2.1.2.2 Simplified Evaluation of the Dipole Matrix Element

The dipole matrix element involving atomic orbitals, $|\alpha\rangle$ and $|\beta\rangle$, on neighboring atoms can be approximated in a very simple form in terms of known[1,11] parameters. These known parameters are the atomic term values (ε_α and ε_β, corresponding to each atomic orbital) and the matrix element of the crystal Hamiltonian between the two atomic orbitals ($V_{\alpha\beta} = \langle\alpha|H|\beta\rangle$). In addition, the two atomic orbitals are assumed to be orthogonal: $\langle\alpha|\beta\rangle = 0$. To obtain the desired dipole matrix element, the eigenstates in the LCAO context of this isolated pair of atomic orbitals will first be constructed. Then, the molecular dipole matrix will be related back to the dipole matrix element between two atomic orbitals.

The eigenvalues are simply given by

$$\left.\begin{matrix}\varepsilon_c \\ \varepsilon_v\end{matrix}\right\} = (\varepsilon_\alpha + \varepsilon_\beta)/2 \pm \sqrt{(\varepsilon_\alpha - \varepsilon_\beta)^2/4 + V_{\alpha\beta}^2} \qquad (15)$$

where the subscript c and v are refer to the conduction and valence, respectively. The eigenstates are written

$$|v\rangle = U_\alpha^v|\alpha\rangle + U_\beta^v|\beta\rangle$$

$$|c\rangle = U_\alpha^c|\alpha\rangle + U_\beta^c|\beta\rangle \qquad (16)$$

and the LCAO coefficients are given by

$$U^v_\alpha = +U^c_\beta = \sqrt{(1 + \alpha_p)/2}$$

$$U^v_\beta = -U^c_\alpha = \sqrt{(1 - \alpha_p)/2} \tag{17}$$

where

$$\alpha_p = [4V^2_{\alpha\beta}/(\varepsilon_\beta - \varepsilon_\alpha)^2 + 1]^{-1/2} \tag{18}$$

and represents the "polarity" of the coupling.

Making use of a general relation[12] among matrix elements between eigenstates,

$$\langle v|\frac{\partial}{\partial x_i}|c\rangle = (m/\hbar^2)(\varepsilon_c - \varepsilon_v)\langle v|x_i|c\rangle \tag{19}$$

the dipole matrix element with a gradient operator is replaced by a matrix element with a position operator. The position matrix element of the two eigenstates is immediately expressed as

$$\langle v|x_i|c\rangle = \sqrt{(1 + \alpha_p)(1 - \alpha_p)}\ (\langle\beta|x_i|\beta\rangle - \langle\alpha|x_i|\alpha\rangle)/2 + \alpha_p\langle\alpha|x_i|\beta\rangle \tag{20}$$

where $|\alpha\rangle$ and $|\beta\rangle$ are assumed to be real which implies that $\langle\beta|x_i|\alpha\rangle = \langle\alpha|x_i|\beta\rangle$. This last term vanishes if the atomic energies of the states are

the same (i.e., $\alpha_p = 0$) or if the two states are symmetric about the midpoint between them. (Note that since the two atomic states are orthogonal, this matrix element in the last term is independent of the origin of coordinates.) As in early treatments,[1] this term is assumed to be zero (the only step in the derivation of the dipole matrix element of two atomic orbitals that is not rigorously justified). Then the first term in Eq. (20) is proportional to the i-th component of the interatomic distance vector, $\vec{d}$,

$$d_i = \langle\beta|x_i|\beta\rangle - \langle\alpha|x_i|\alpha\rangle \tag{21}$$

permitting Eq. (20) to be written as

$$\langle v|x_i|c\rangle = \sqrt{1 - \alpha_p^2}\, d_i/2 \tag{22}$$

The gradient matrix element of two eigenstates in Eq. (19) is expanded, in a similar fashion to Eq. (20), as

$$\langle v|\frac{\partial}{\partial x_i}|c\rangle = \sqrt{1 - \alpha_p^2}\,\left(\langle\beta|\frac{\partial}{\partial x_i}|\beta\rangle - \langle\alpha|\frac{\partial}{\partial x_i}|\alpha\rangle\right)/2 + \langle\alpha|\frac{\partial}{\partial x_i}|\beta\rangle \tag{23}$$

where a partial integration has been used to show that $\langle\beta|\partial/\partial x_i|\alpha\rangle = -\langle\alpha|\partial/\partial x_i|\beta\rangle$ in the last term. Additionally, the same partial integration shows that both $\langle\alpha|\partial/\partial x_i|\alpha\rangle$ and $\langle\beta|\partial/\partial x_i|\beta\rangle$ vanish, so Eq. (23) becomes

$$\langle v|\frac{\partial}{\partial x_i}|c\rangle = \langle\alpha|\frac{\partial}{\partial x_i}|\beta\rangle \quad . \tag{24}$$

Substituting Eqs. (22) and (23) back into Eq. (19) and solving for the dipole matrix element between atomic states gives

$$\langle\alpha|\frac{\partial}{\partial x_i}|\beta\rangle = (m/\hbar^2)(\varepsilon_c - \varepsilon_v)\sqrt{1 - \alpha_p^2}\, d_i/2 \quad . \tag{25}$$

This expression further simplifies by using Eqs. (15) and (18) to give $(\varepsilon_c - \varepsilon_v) = 2V_{\alpha\beta}\sqrt{1 - \alpha_p^2}$ which yields

$$\langle\alpha|\frac{\partial}{\partial x_i}|\beta\rangle = -(m/\hbar^2)V_{\alpha\beta}d_i \tag{26}$$

for the final form of the dipole matrix element involving two atomic orbitals.

2.1.2.3 Simplified Linear Susceptibility Formula

This form for the dipole matrix elements (Eq. (26)) can be utilized in the tight-binding formulation of the first-order susceptibility (Eq. (14)) when atomic orbitals are substituted for the Wannier functions. The energies in the denominator of Eq. (14) can be adequately represented by the eigenvalues of a pair of coupled states in Eq. (15) and the resulting linear susceptibility is written

$$\chi_{ij}^{(1)} = \frac{4e^2}{\Omega} \sum_{\alpha,\beta}^{(nn)} \frac{V_{\alpha\beta}^2\, d_i d_j}{[(\varepsilon_\beta - \varepsilon_\alpha)^2 + 4V_{\alpha\beta}^2]^{3/2}} \tag{27}$$

where the summation is over nearest neighbor atomic orbitals.

2.1.2.4 Applications

This formula is directly applicable to any specific material with all the necessary parameters known once the crystal geometry has been determined. The only complication is the possibility of a large number of terms entering the summation over atomic orbitals. Even further simplifications can result if assumptions about the electronic band structure for the particular compounds of interest are incorporated at this point.

Consider, for example, the alkali-halides. First, note that the covalent energy is always much less than the polar energy for all pairs of s and p states. Consequently, the $V_{\alpha\beta}$ term in the denominator of Eq. (27) is negligible. Also, the only important atomic states which enter are the s-state on the alkali atom and the p-state on the halide atom. This is because the energy difference between other pairs of nearest neighbor atomic states is significantly larger. Finally, in a principle axis coordinate system, the interatomic distance vectors are directed along one of the principle axes which means that $d_i d_j = d^2 = a^2/4$ only when $i = j$. Since there are six nearest neighbors surrounding each of the two atoms in the primitive cell,

$$x_{ii}^{(1)} = \frac{4e^2\hbar^4\eta_{sp\sigma}^2}{m^2 d^5(\varepsilon_s - \varepsilon_p)^3} \tag{28}$$

where $\Omega = 2d^3$ has been used and numerical values for the coefficient, $\eta_{sp\sigma}$, are given in Ref. 1. This prediction has been compared to experiment elsewhere.[1]

The case of the binary semiconductors is almost as simple. Here, hybrid orbitals are formed and the interatomic matrix element, which is replaced by the covalent energy (V_2), is no longer negligible and gives

$$x_{ii}^{(1)} = \frac{\sqrt{3}e^2V_2^2}{64d(V_2^2 + V_3^2)^{3/2}} \tag{29}$$

with $\Omega = 2a^3 = 128\ d^3/3\sqrt{3}$ for four hybrid bonds and where $V_2 = -3.22\ \hbar^2/(md^2)$ and $V_3 = (\varepsilon_s^c + 3\varepsilon_p^c - \varepsilon_s^a - 3\varepsilon_p^a)/8$ are the covalent and polar energies, respectively, as previously defined.[11]

2.1.2.5 Dipole Moments

Harrison has utilized the concept of a dipole moment of a chemical bond when considering the susceptibility of tetrahedral semiconductors. The i^{th} vector component of this dipole moment has been written as

$$p_i = ed_i\alpha_p \tag{30}$$

where $\alpha_p = V_3/\sqrt{V_2^2 + V_3^2}$ is the polarity of the bond. Then, the total induced polarization density is just the summation over bonds of each dipole moment averaged over the volume occupied by the bonds. This dipole moment concept can also be employed within the context of the above formalism. Here, the "dipole moment" represents the induced coupling between two atomic orbitals and can be written as in Eq. (30) but with the "polarity" given by Eq. (18). The connection between the bond dipole moment and the susceptibility can be established rigorously as follows. As before, the total induced polarization density is

$$P_i = \frac{1}{\Omega}\sum_{cs} p_i \tag{31}$$

where Ω is the volume occupied by the coupled states. Now, with reference to Eq. (5), each dipole moment is written as a Taylor's series expansion of the electric field and Eq. (31) becomes

$$P_i = \frac{1}{\Omega}\sum_{cs}\left[\sum_j \frac{\partial p_i}{\partial E_j}E_j + \frac{1}{2}\sum_{jk}\frac{\partial^2 p_i}{\partial E_j \partial E_k}E_jE_k + \cdots\right] \tag{32}$$

where $\partial p_i/\partial E_j$ is the i-th component of the contribution to the first-order susceptibility from each dipole moment. After interchanging the summation over coupled states with summations over vector components in Eq. (32) and comparing back to Eq. (5), the first-order susceptibility is then identified as

$$\chi_{ij}^{(1)} = \frac{1}{\Omega} \sum_{cs} \frac{\partial p_i}{\partial E_j} \quad . \tag{33}$$

To verify this expression, one can carry out the differentitation according to the chain-rule:

$$\frac{\partial p_i}{\partial E_j} = \left(\frac{\partial d_i}{\partial E_j}\right)\left(\frac{\partial p_i}{\partial d_i}\right) + \underbrace{\left(\frac{\partial V_{\alpha\beta}}{\partial E_j}\right)\left(\frac{\partial p_i}{\partial V_{\alpha\beta}}\right)} + \left(\frac{\partial \varepsilon_{\alpha\beta}}{\partial E_j}\right)\left(\frac{\partial p_i}{\partial \varepsilon_{\alpha\beta}}\right)$$

$$\underbrace{\qquad\qquad\qquad\qquad\qquad\qquad}$$

$$\frac{-2V_{\alpha\beta}}{d^2} \sum_{m=1}^{3} \left(\frac{\partial d_m}{\partial E_j}\right) d_m \quad \left(\frac{\partial p_i}{\partial V_{\alpha\beta}}\right) \tag{34}$$

where the independent variables are d_i, $V_{\alpha\beta} \sim 1/d^2$ and $\varepsilon_{\alpha\beta} = (\varepsilon_\alpha - \varepsilon_\beta)$. If the frequency of the an optical electric field is above the Reststrahl vibrational frequencies, the atoms do not respond and hence the change in the m-th component of the interactomic distance vector with respect to this optical field, $(\partial d_m/\partial E_j)$, is zero. Consequently, only the last term in Eq. (34) is nonzero. Note that the energy difference, $\varepsilon_{\alpha\beta}$, is modified by the dipole energy, $-e\vec{d}\cdot\vec{E}$, when the optical field is applied. This last term is easily evaluated and the resulting linear susceptibility is, of course, identical to Eq. (27).

2.1.3 Higher-Order Susceptibilities

The various second- and third-order susceptibilities can be treated in a similar fashion to the linear susceptibility in Eq. (33). As a note of caution, the particular Taylor's series expansion (as used in Eq. (32)) must reflect the experiment being considered. For example, in second harmonic generation, there is only one electric field which is the optical field and the Taylor's series expansion in three independent variables (the three components of this optical field) as written in Eq. (32) is appropriate. Then, the second harmonic susceptibility is immediately recognized as

$$\chi_{ijk}^{SHG} = \frac{1}{2\Omega} \sum_{cs} \frac{\partial^2 p_i}{\partial E_j \partial E_k} \tag{35}$$

where the full tensor notation has been explicitly retained. Again, performing the differentiation is relatively trivial when the change in interatomic distance vector is zero, as it is for the case of second harmonic generation. The result can be written

$$\chi_{ijk}^{SHG} = \frac{6e^3}{\Omega} \sum_{\alpha\beta}^{(nn)} \frac{(\varepsilon_\beta - \varepsilon_\alpha) V_{\alpha\beta}^2 d_i d_j d_k}{[(\varepsilon_\beta - \varepsilon_\alpha)^2 + 4V_{\alpha\beta}^2]^{5/2}} \tag{36}$$

and is obviously symmetric in indices, i, j and k which is consistent with Kleinman's symmetry condition.[2]

2.1.4 Electro-Optic Susceptibility

As another example, consider the linear dc (Pockel's) effect. The electro-optic susceptibility is related to the changes induced in each dipole moment by both the optical and dc electric fields. This can be seen mathematically by writing out the Taylor's series expansion for the i-th vector

component of the dipole moment in terms of the six independent variables (which correspond to the three components of both the optical and dc electric fields):

$$p_i(\vec{E}^{opt},\vec{E}^{dc}) = p_i(\vec{E}^{opt}=0,\vec{E}^{dc}=0) + \sum_{j=1}^{3}\left(\frac{\partial p_i}{\partial E_j^{opt}}\right)E_j^{opt} + \sum_{j=1}^{3}\left(\frac{\partial p_i}{\partial E_j^{dc}}\right)E_j^{dc}$$

$$+ \left(\frac{1}{2}\right)\sum_{j=1}^{3}\sum_{k=1}^{3}\left(\frac{\partial^2 p_i}{\partial E_j^{opt}\partial E_k^{opt}}\right)E_j^{opt}E_k^{opt} + \left(\frac{1}{2}\right)\sum_{j=1}^{3}\sum_{k=1}^{3}\left(\frac{\partial^2 p_i}{\partial E_j^{dc}\partial E_k^{dc}}\right)E_j^{dc}E_k^{dc}$$

$$+ (1)\sum_{j=1}^{3}\sum_{k=1}^{3}\left(\frac{\partial^2 p_i}{\partial E_j^{opt}\partial E_k^{opt}}\right)E_j^{opt}E_k^{dc} + \ldots \qquad (37)$$

The contributions from each dipole moment to the electro-optic susceptibility arise from terms proportional to $E_j^{opt}E_k^{dc}$, i.e., the last summation in Eq. (37). Consequently, the electro-optic susceptibility can be written

$$\chi_{ikj}^{EO} = \frac{1}{\Omega}\sum_{cs}\frac{\partial^2 p_i}{\partial E_j^{opt}\partial E_k^{dc}} \qquad (38)$$

where the summation is over all nearest-neighbor coupled atomic states. The derivative in Eq. (38) can be expressed in terms of a set of known parameters by carrying out the differentiation on Eq. (30) as follows. The i-th component of the dipole moment in Eq. (30) is a function of the variables d_i, $V_{\alpha\beta}$ and $\varepsilon_{\alpha\beta}$. We apply the chain rule to convert the derivative with respect to E_j^{opt} into separate derivatives with respect to these three variables. Noting that d_i and $V_{\alpha\beta}$ are constant in the presence of a high frequency

optical field, E_j^{opt}, we find that the optically-induced change in the dipole moment is[1]

$$\frac{\partial p_i}{\partial E_j^{opt}} = \left(\frac{\partial \varepsilon_{\alpha\beta}}{\partial E_j^{opt}}\right)\left(\frac{\partial p_i}{\partial \varepsilon_{\alpha\beta}}\right) = \frac{4e^2 d_i d_j V_{\alpha\beta}^2}{(\varepsilon_{\alpha\beta}^2 + 4V_{\alpha\beta}^2)^{3/2}} \quad . \tag{39}$$

This represents the contribution of each dipole moment to the first-order susceptibility. By contrast, the dc electric field induces an additional change in the dipole moment, involving terms in which include the lattice response. Using the chain rule with four variables (d_i, d_j, $V_{\alpha\beta}$ and $\varepsilon_{\alpha\beta}$), this second-order effect becomes

$$\frac{\partial}{\partial E_k^{dc}}\left(\frac{\partial p_i}{\partial E_j^{opt}}\right) = \left[\left(\frac{\partial d_i}{\partial E_k^{dc}}\right)\frac{\partial}{\partial d_i} + \left(\frac{\partial d_j}{\partial E_k^{dc}}\right)\frac{\partial}{\partial d_j} + \underbrace{\left(\frac{\partial V_{\alpha\beta}}{\partial E_k^{dc}}\right)\frac{\partial}{\partial V_{\alpha\beta}}} + \left(\frac{\partial \varepsilon_{\alpha\beta}}{\partial E_k^{dc}}\right)\frac{\partial}{\partial \varepsilon_{\alpha\beta}}\right]$$

$$\frac{4e^2 d_i d_j}{(\varepsilon_{\alpha\beta}^2 + 4V_{\alpha\beta}^2)^{3/2}} \overbrace{\frac{-2V_{\alpha\beta}}{d^2}\sum_{m=1}^{3} d_m \left(\frac{\partial d_m}{\partial E_k^{dc}}\right)} \tag{40}$$

The evaluation of the lattice response to the dc electric field (i.e., the factors, $\partial d_n/\partial E_k^{dc}$ will be treated as a separate problem in Section 2.1.5. Then, the remaining derivatives in Eq. (40) can be expressed entirely in terms of known parameters, assuming the crystal structure has been specified. Performing these differentiations yields

$$\chi_{ikj}^{EO} = \frac{4e^2}{\Omega}\sum_{\alpha,\beta}^{(nn)} \frac{V_{\alpha\beta}^2}{(\varepsilon_{\alpha\beta}^2 + 4V_{\alpha\beta}^2)^{5/2}}\left\{3ed_i d_j d_k \varepsilon_{\alpha\beta} + \sum_{m=1}^{3}\left(\frac{\partial d_m}{\partial E_k^{dc}}\right)\left[(\varepsilon_{\alpha\beta}^2 + 4V_{\alpha\beta}^2)\right.\right.$$

$$\left.\left.(d_i \delta_{jm}) + d_j \delta_{im}) + 4(2V_{\alpha\beta}^2 - \varepsilon_{\alpha\beta}^2) d_i d_j d_m/d^2\right]\right\} \tag{41}$$

where $\delta_{\ell m}$ is the Kronecker delta, $\varepsilon_{\alpha\beta} = (\varepsilon_\alpha - \varepsilon_\beta)^2$ and the first summation is over coupled nearest-neighbor atomic orbitals.

2.1.5 Lattice Contribution to the Electro-Optic Effect

First, the dynamical matrix method will be used to describe the lattice equations of motion in three dimensions for a generalized crystal structure. This method will employ only nearest-neighbor bond-stretching and bond-bending force constants[1] for simplicity. Only the phonon modes at zero wavevector will enter the calculation of the electro-optic effect; however the entire lattice spectrum is investigated in order to test this force-constant model. Then the force on each atom in the unit cell, due to the dc electric field, will be quantified by assigning an effective charge to each atom. Hence, the displacement, in response to the dc electric field, of every atom in the unit cell will be determined.

2.1.5.1 Lattice Equations of Motion

Consider a crystal consisting of N atoms per unit cell. When the lattice is perturbed (by a dc electric field, for example), each atom in the unit cell will undergo elastic motion in response to this perturbation. This elastic motion can be modelled using a nearest-neighbor formalism similar to that used in Eq. (41). In this model each atom in the unit cell experience two types of forces when it is displaced from its equilibrium position. The first is a bond-stretching force and is simply due to the radial change in interatomic distance between the m-th atom in the unit cell and each of its nearest neighbors (atom ℓ), as shown in Fig. 1a. The second type force is a bond-bending force and is due to the change in bond angles. For each atom in the unit cell, there are two different kinds of bond angles to consider; one involves two first-neighbors (atoms ℓ and n) while the other involves a first-nearest neighbor (atom n) and a second-nearest neighbor (atom m′). These two contributions to the elastic motion of the m-th atom in the unit cell are illustrated in Figs. 1b and 1c, respectively.

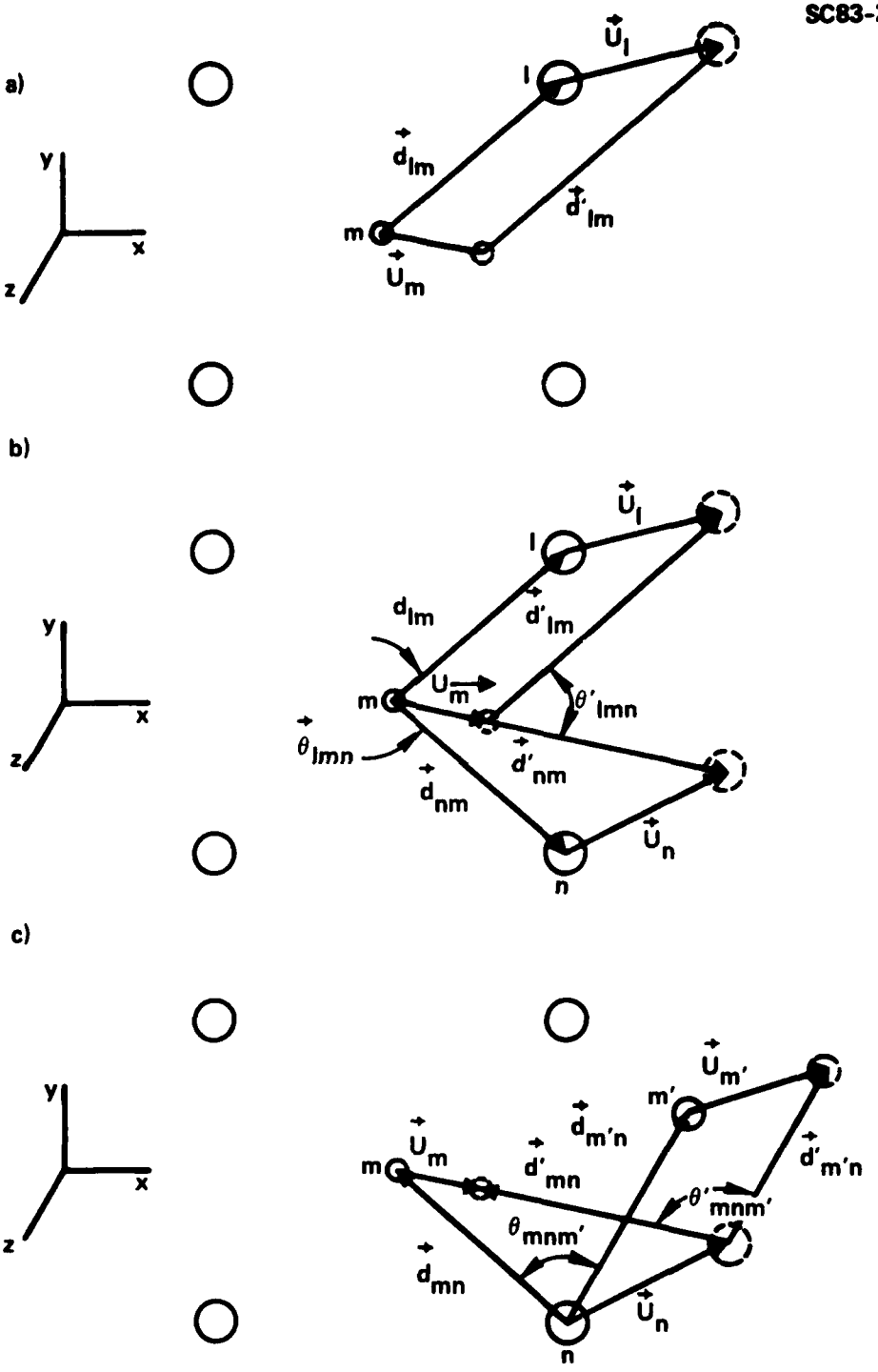

Fig. 1 Equilibrium and non-equilibrium atomic configurations of nearest neighbor atoms for: (a) bond-stretching forces, (b) bond-bending forces with two first-nearest neighbors, and (c) bond-bending forces with a first- and a second-nearest neighbor.

The potential energy associated with the bond-stretching between atoms m and ℓ can be written

$$\varepsilon_{\ell m} = \frac{1}{2} C_0 \Delta d^2_{\ell m}/d^2_{\ell m} \tag{42}$$

where C_0 is defined[1] as the radial force constant, $\Delta d_{\ell m}$ is the change in magnitude of the interatomic distance and $d_{\ell m}$ is the equilibrium interatomic distance. Similarly, the potential energy associated with the bond-bending between atom m and nearest neighbor atoms ℓ and n is

$$\varepsilon_{\ell m n} = \frac{1}{2} C_1 \Delta\theta^2_{\ell m n} \tag{43}$$

where C_1 is defined[1] as the angular force constant and, $\Delta\theta_{\ell m}$ is the change in the bond angle. Finally, the potential energy associated with the bond-bending between atom m, first-nearest neighbor atom n and second-nearest neighbor atom m′ can be written in a fashion analogous to Eq. (43).

Using these three contributions to the potential energy, the total force on the m-th atom in the unit cell becomes

$$\vec{F}_m = -\sum_{\ell} \vec{\nabla}\varepsilon_{\ell m} - \sum_{\ell}\sum_{n\neq\ell} \vec{\nabla}\,\varepsilon_{\ell m n} - \sum_{n}\sum_{m'\neq\ell} \vec{\nabla}\varepsilon_{m n m'}$$

$$= -\frac{1}{2}\sum_{\ell} (C_0)_{\ell m} \vec{\nabla}(\Delta d^2_{\ell m})/d^2_{\ell m} - \frac{1}{2}\sum_{\ell}\sum_{n\neq\ell} (C_1)_{\ell m n} \vec{\nabla}(\Delta\theta^2_{lmn})$$

$$-\frac{1}{2}\sum_{n}\sum_{m'\neq m} (C_1)_{m n m'} \vec{\nabla}(\Delta\theta^2_{m n m'}) \tag{44}$$

where the summation for the bond-stretching contribution is over all nearest neighbor atoms (ℓ), the summation for the first bond-bending contribution is over all combinations of nearest-neighbor pairs (ℓ and n) and the summation for the second bond-bending contribution includes each first-nearest neighbor atom (n) paired with all of its first-nearest-neighbor atoms (m′) excluding atom m. The gradient in Eq. (44) is with respect to the displacement vector associated with atom m. Note that there is only one set of angular force constants for $(C_1)_{\ell mn}$ and $(C_1)_{mnm'}$. The differentiations indicated in Eq. (44) can be carried out in a straight-forward manner. First, for the bond-stretching contribution, the change in magnitude of the interatomic distance can be written explicitly as a function of the displacement vector, $\vec{u}_m$, of atom m:

$$\Delta d_{\ell m} = \vec{d}'_{\ell m} - \vec{d}_{\ell m} = (\vec{d}_{\ell m} \cdot \vec{u}_{\ell m})/d^2_{\ell m} \qquad (45)$$

where a binomial expansion has been used and only terms up to first order in the displacements were kept. Here and throughout a short-hand notation is used for the difference between two vectors, e.g., the displacement vectors in Eq. (45) enter as $\vec{u}_{\ell m} \equiv \vec{u}_\ell - \vec{u}_m$. Then the gradient of $\Delta d_{\ell m}$ is simply expressed as

$$\vec{\nabla}(\Delta d^2_{\ell m})/d^2_{\ell m} = -2\vec{d}_{\ell m}(\vec{d}_{\ell m} \cdot \vec{u}_{\ell m})/d^4_{\ell m} \quad . \qquad (46)$$

The bond-bending contributions are considerably more complicated, mainly due to the algebra. The change in bond angle can be related to the displacement vectors, $\vec{u}_m$, as follows. In the equilibrium configuration, the cosine of the bonding angle is

$$\cos \theta_{\ell mn} = (\vec{d}_{\ell m} \cdot \vec{d}_{nm})/(d_{\ell m} d_{nm}) \tag{47}$$

written in terms of the interatomic distance vectors. For the perturbed configuration, the cosine of the bonding angle becomes

$$\cos \theta'_{\ell mn} = [\vec{d}_{\ell m} \cdot \vec{d}_{nm}(1 - \vec{d}_{\ell m} \cdot \vec{u}_{\ell m}/d^2_{\ell m} - \vec{d}_{nm} \cdot \vec{u}_{nm}/d^2_{nm})$$

$$+ \vec{d}_{\ell m} \cdot \vec{u}_{nm} + \vec{d}_{nm} \cdot \vec{u}_{\ell m}]/(d_{\ell m} d_{nm}) \tag{48}$$

again using the binomial expansion and discarding terms second order or higher in the displacements. The small change in bond angle is related to the difference in the two cosines (Eqs. (47) and (48)) via the definition of the derivative for the cosine. This change in angle can then be written as

$$\Delta\theta_{\ell mn} = -[(\hat{d}_{nm} - \hat{d}_{\ell m} \cos \theta_{\ell mn}) \cdot \vec{u}_{\ell m}/d_{\ell m} + (\hat{d}_{\ell m} - \hat{d}_{nm} \cos \theta_{\ell mn})$$

$$\cdot \vec{u}_{nm} d_{nm}]/\sin \theta_{\ell mn} \tag{49}$$

where $\hat{d}_{\ell m}$ and $\hat{d}_{nm}$ are unit vectors directed between nearest-neighbor atoms. Finally, the two gradients with respect to the displacement vector, $\vec{u}_m$, of the square of the change in bond angle (after a fair amount of algebra) becomes

$$\vec{\nabla}(\Delta\theta^2_{\ell mn}) = \left(\frac{+2}{\sin^2\theta_{\ell mn} d_{\ell m} d_{nm}}\right)\left\{\left[\frac{d^2_{nm}}{d^2_{\ell m}}\vec{d}_{\ell m}\cos^2\theta_{\ell mn} - \frac{d_{nm}}{d_{\ell m}}(\vec{d}_{\ell m} + \vec{d}_{nm})\cos\theta_{\ell mn} + \vec{d}_{nmn}\cos^2\theta_{\ell mn}\right](\vec{d}_{\ell m}\cdot\vec{u}_{\ell m}) + \left[\vec{d}_{\ell m} + \vec{d}_{nm} - \frac{d_{nm}}{d_{\ell m}}\vec{d}_{\ell m}\cos\theta_{\ell mn} - \frac{d_{\ell m}}{d_{nm}}\vec{d}_{nm}\cos\theta_{\ell mn}\right](\vec{d}_{nm}\cdot\vec{u}_{\ell m} + \vec{d}_{\ell m}\cdot\vec{u}_{nm}) + \left[\frac{d^2_{\ell m}}{d^2_{nm}}\vec{d}_{nm}\cos^2\theta_{\ell mn} - \frac{d_{\ell m}}{d_{nm}}(\vec{d}_{\ell m} + \vec{d}_{nm})\cos\theta_{\ell mn} + \vec{d}_{\ell m}\cos^2\theta_{\ell mn}\right](\vec{d}_{nm}\cdot\vec{u}_{nm})\right\} \quad (50)$$

for the case of two first-nearest neighbors to atom m and

$$\vec{\nabla}(\Delta\theta^2_{mnm'}) = \left(\frac{-2}{\sin^2\theta_{mnm'} d^2_{mn} d^2_{m'n}}\right)\left\{\left[\frac{d^2_{m'n}}{d^2_{mn}}\vec{d}_{mn}\cos^2\theta_{mnm'} - \frac{d_{m'n}}{d_{mn}}\vec{d}_{m'n}\cos\theta_{mnm'}\right](\vec{d}_{mn}\cdot\vec{u}_{mn}) + \left[\vec{d}_{m'n} - \frac{d_{m'n}}{d_{mn}}\vec{d}_{mn}\cos\theta_{mnm'}\right](\vec{d}_{m'n}\cdot\vec{u}_{mn} + \vec{d}_{mn}\cdot\vec{u}_{m'n}) + \left[\vec{d}_{mn}\cos^2\theta_{mnm'} - \frac{d_{mn}}{d_{m'n}}\vec{d}_{m'n}\cos\theta_{mnm'}\right](\vec{d}_{m'n}\cdot\vec{u}_{m'n})\right\} \quad (51)$$

for the case of one first-nearest neighbor and one second-nearest neighbor to atom m.

By substituting Eqs. (46), (50), and (51) back into Eq. (44), the generalized equation of motion for the m-th atom in the unit cell is obtained. While this equation of motion appears to be rather complicated on the surface, closer inspection reveals that most of the factors (e.g., and $d_{\ell m}$, $\theta_{\ell mn}$ and $\theta_{mnm'}$) are directly related to the unperturbed crystal geometry and also that this equation is nonlinear in the displacements. The only parameters which are not immediately in hand are the set of bond-stretching and bond-bending force constants ($(C_0)_{\ell m}$ and $(C_1)_{\ell mn}$ respectively). For simple crystals, such as the binary semiconductors, the bonds are all identical (or nearly so) and only a single pair of numbers is needed for C_0 and C_1. In more complex crystal structures, the bonds are no longer equivalent and the degeneracy in the force constants is broken. Methods for determining these force constants have been, and are still being, investigated.[13] Consequently, for the problem being addressed here, it is assumed that these force constants are known.

2.1.5.2 Lattice Dispersion Curves

Now consider the complete set of equations of motion for each x-y-z component, of each m-th atom in the unit cell. By assuming that all of these motions can be described by Hooke's law (and that each atom undergoes simple harmonic motion in response to any perturbation), the force on the m-th atom in the unit cell can be written as

$$\vec{F}_m = -M_m \omega^2 \vec{u}_m \qquad (52)$$

where M_m is the mass of the m-th atom, ω is the frequency of vibration and $\vec{u}_m$ is the displacement vector of the m-th atom from its equilibrium position,

as before. Equating these components of the force with those derived from the equations of motion (Eq. (44)) gives a set of 3N coupled linear equations in the terms of the 3N components of the atomic displacement vectors. Here N is the number of atoms in the unit cell.

There is perhaps, one additional complication to the equations of motion that has been omitted up to this point. That is the constraint imposed by the periodic boundary conditions associated with the crystal lattice. These boundary conditions dictate that the vector displacements, $\vec{u}_m$ and $\vec{u}_{m'}$, of two atoms located at equivalent lattice sites in two different unit cells must be related by a phase factor corresponding to the periodicity of the lattice, i.e., $\vec{u}_{m'} = \vec{u}_m \exp(i\vec{K} \cdot \vec{d}_{mm'})$. One simple procedure for assigning the phase factors properly is to multiply each component of the displacement vectors, $\vec{u}_m$, by $\exp(i\vec{K} \cdot \vec{r}_m)$ where $\vec{r}_m$, is the vector distance from some fixed origin to the m-th atom in the appropriate unit cell.

The lattice dynamical matrix, with dimensions of 3N × 3N, corresponding to the right-hand side of Eq. (44) can be expressed in terms of the coefficients given in Eqs. (46), (50), and (51) along with the phase factors discussed in the preceeding paragraph. The matrix element, Φ_{m_i,k_j}, is defined as the coefficient of the j-th component of the k-th displacement vector associated with the i-th component of the force on the m-th atom in the unit cell. It can be written

$$\Phi_{m_i,k_j} = -\frac{1}{M_m} e^{-i\vec{K}\cdot\vec{r}_m}\left[\sum_{\ell} A_{\ell mi} d_{\ell mj}\left(\delta_{mk} e^{i\vec{K}\cdot\vec{r}_m} - \delta_{\ell k} e^{i\vec{K}\cdot\vec{r}_\ell}\right)\right.$$

$$\left. + \sum_{\ell}\sum_{n\neq\ell} B_{\ell mn}\left\{C_{\ell mni} d_{\ell mj}\left(\delta_{\ell k} e^{i\vec{K}\cdot\vec{r}_\ell} - \delta_{mk} e^{i\vec{K}\cdot\vec{r}_m}\right)\right.\right.$$

$$+ D_{\ell mn i} d_{mnj} \left(\delta_{\ell k} e^{i\vec{K}\cdot\vec{r}_\ell} - \delta_{mk} e^{i\vec{K}\cdot\vec{r}_m}\right)$$

$$+ E_{\ell mni} d_{nmj} \left(\delta_{nk} e^{i\vec{K}\cdot\vec{r}_n} - \delta_{mk} e^{i\vec{K}\cdot\vec{r}_m}\right)$$

$$+ F_{\ell mni} d_{\ell mj} \left(\delta_{nk} e^{i\vec{K}\cdot\vec{r}_n} - \delta_{mk} e^{i\vec{K}\cdot\vec{r}_m}\right) \Bigg\}$$

$$+ \sum_n \sum_{m' \neq m} G_{mnm'} \Bigg\{ H_{mnm'i} d_{mnj} \left(\delta_{mk} e^{i\vec{K}\cdot\vec{r}_m} - \delta_{nk} e^{i\vec{K}\cdot\vec{r}_n}\right)$$

$$+ I_{mnn'i} d_{m'nj} \left(\delta_{mk} e^{i\vec{K}\cdot\vec{r}_m} - \delta_{nk} e^{i\vec{K}\cdot\vec{r}_n}\right)$$

$$+ J_{mnm'i} d_{m'nj} \left(\delta_{m'k} e^{i\vec{K}\cdot\vec{r}_{m'}} - \delta_{nk} e^{i\vec{K}\cdot\vec{r}_n}\right)$$

$$+ K_{mnm'i} d_{mnj} \left(\delta_{m'k} e^{i\vec{K}\cdot\vec{r}_{m'}} - \delta_{nk} e^{i\vec{K}\cdot\vec{r}_n}\right) \Bigg\} \Bigg] \qquad (53)$$

where $\delta_{\ell m}$ is the Kronecker delta and the overall normalization, $\exp(-i\vec{k}\cdot\vec{r}_m)/M_n$, is the mass and phase factor associated with Eq. (52). The various coefficients in Eq. (53) are defined by:

$$A_{\ell mi} = -(C_0)_{\ell m} d_{\ell mi} / d^4_{\ell m} \qquad (54)$$

$$B_{\ell mn} = +(C_1)_{\ell mn}/(\sin^2\theta_{\ell mn} d^2_{\ell n} d^2_{nm}) \tag{55}$$

$$C_{\ell mni} = E_{nm\ell i} = \frac{d^2_{nm}}{d^2_{\ell m}} d_{\ell mi} \cos^2\theta_{\ell mn} - \frac{d_{nm}}{d_{\ell m}} (d_{\ell mi} + d_{nmi}) \cos\theta_{\ell mn} + d_{nmi} \cos^2\theta_{\ell mn} \tag{56}$$

$$D_{\ell mni} = F_{\ell mni} = d_{\ell mi} + d_{nmi} - \frac{d_{nm}}{d_{\ell m}} d_{\ell mi} \cos\theta_{\ell mn} - \frac{d_{\ell m}}{d_{nm}} d_{nmi} \cos\theta_{\ell mn} \tag{57}$$

$$G_{mnm'} = -(C_1)_{mnm'}/(\sin^2\theta_{mnm'} d^2_{mn} d^2_{m'n}) \tag{58}$$

$$H_{mnm'i} = \frac{d^2_{m'n}}{d^2_{mn}} d_{mni} \cos^2\theta_{mnm'} - \frac{d_{m'n}}{d_{mn}} d_{m'ni} \cos\theta_{mnm'} \tag{59}$$

$$I_{mnm'i} = K_{mnm'i} = d_{m'ni} - \frac{d_{m'n}}{d_{mn}} d_{mni} \cos\theta_{mnm'} \tag{60}$$

$$J_{mnm'j} = d_{mni} \cos^2\theta_{mnm'} - \frac{d_{mn}}{d_{m'n}} d_{m'ni} \cos\theta_{mnm'} \tag{61}$$

where the triple subscript notation represents one specific component of the vector difference (e.g, $d_{\ell mj} = (\vec{d}_\ell - \vec{d}_m)_j = (\vec{d}_\ell)_j - (\vec{d}_m)_j$). The equations of motion can now be written in matrix notation as

$$\sum_{k=1}^{N} \sum_{j=1}^{3} \Phi_{m_i,k_j} (\vec{u}_k)_j = (-M_m\omega^2)(\vec{u}_m)_i \qquad (62)$$

which has the form of an eigenvalue equation where $(-M_m\omega^2)$ is the eigenvalue and $(\vec{u}_m)_i$ is one component of the eigenvector. This eigenvalue problem can be solved by numerically diagonalizing the dynamical matrix at any given wavevector and the solution results in a set of lattice dispersion curves (ω vs K) associated with the 3N eigenvalues. In addition, the 3N normal vibrational modes correspond to the 3N eigenvectors found during the diagonalization process. The dynamical matrix elements (Eq. (53)) could be divided by $\sqrt{M_m M_k}$ instead of $-M_m$ to put the eigenvalue equation in Hermitian form; then the eigenvectors must be multiplied by $\sqrt{M_m}$ to obtain the components of the actual displacement vectors associated with the normal modes. It should be emphasized that this procedure is applicable to any arbitrary crystal geometry, with the only limitation being a computational one due to an unreasonably large number of atoms per unit cell.

The above formalism has been tested on GaAs, a zincblende semiconductor. Using values for the force constants of C_0 = 47.4 eV and C_1 = 2.3 eV gives the dispersion curves shown in Fig. 2. This result appears to exactly reproduce Fig. 9-2 of Reference 1. A more detailed application was performed on the wurtzite semiconductor, CdS, with C_0 = 40 eV and C_1 = 1 eV. First, the forces and motion were assumed to be constrained to the x-direction exclusively. The resulting dispersion curves are given in Fig. 3. Analytical expressions have been derived at K = 0 in order to check these curves: ω = 0 for the acoustical mode and

$$\omega^2 = \left(\frac{1}{M_1} + \frac{1}{M_2}\right)(C_0 + 8C_1) \qquad (63)$$

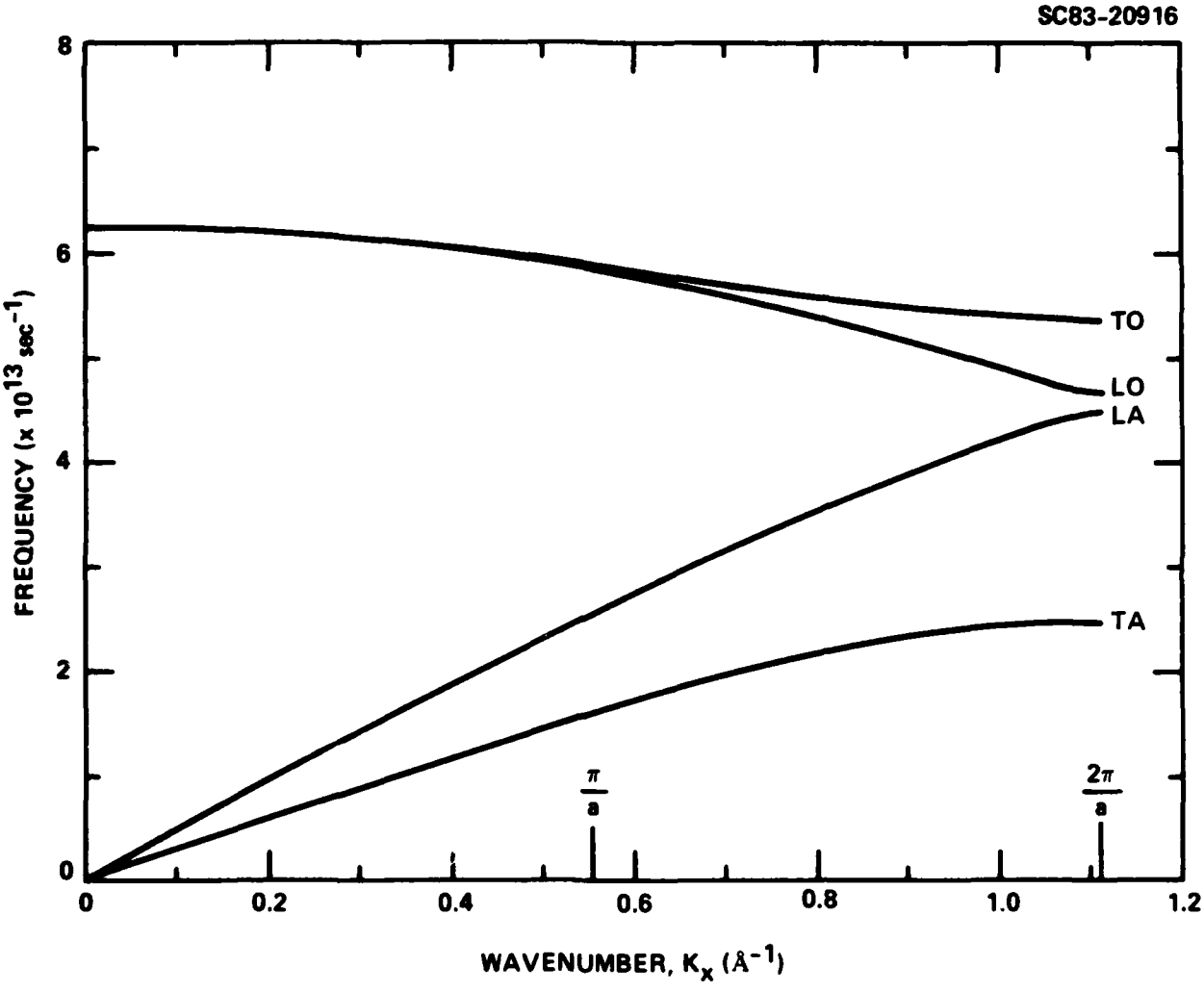

Fig. 2 Lattice dispersion curves for GaAs.

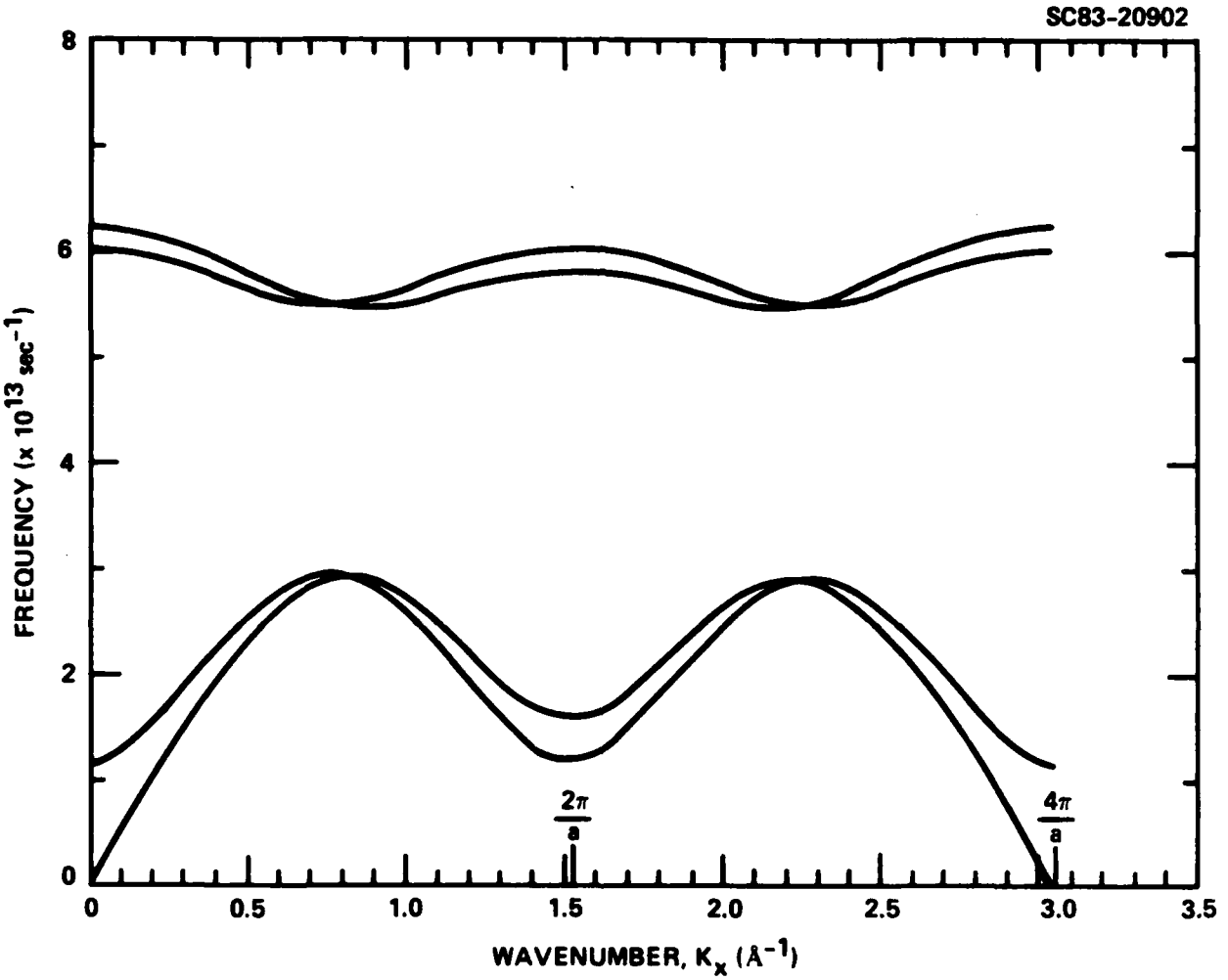

Fig. 3 Lattice dispersion curves for CdS with displacements only along x.

$$\omega^2 \approx -\left(\frac{1}{M_1} + \frac{1}{M_2}\right)\left(C_0 + \frac{13}{2} C_1 - \frac{9M_1M_2}{(M_1 + M_2)^2} C_1\right) \tag{64}$$

$$\omega^2 \approx 9C_1/(M_1 + M_2) \tag{65}$$

for the optical modes. The appearance of this low frequency optical mode, involving only the C_1 force constant, corresponds to pairs of adjacent planes of CdS atoms shearing with respect to each other. Finally, the complete dynamical matrix for CdS, allowing all three degrees of freedom, was diagonalized for the same set of force constants (C_0 = 40 eV and C_1 = 1 eV) and the resulting dispersion curves are given in Fig. 4.

2.1.5.3 Lattice Response to a dc Electric Field

The same dynamical matrix, which was used to determine the lattice dispersion curves (Eq. (62)), can be manipulated to give the response of the crystal lattice to an external dc electric field. The dc field implies using the dynamical matrix at zero wave-vector (K = 0). In order to find the perturbed crystal geometry, the component of force on the right-hand-side of Eq. (40) is replaced with the i-th component of the force exerted by the dc electric field on the m-th atom in the unit cell. The resulting set of linear equations can be written as

$$\sum_{k=1}^{N} \sum_{j=1}^{3} \Phi_{m_i, k_j} (\vec{u}_k)_j = e(e^*_T)_{m_i} E_i \tag{66}$$

where again e is the electronic charge, $(e^*_T)_{m_i}$ is the transverse effective charge corresponding to the m_i-th normal lattice vibrational mode and E_i is the i-th component of the applied dc electric field. This results in only 3N-3 independent equations with 3N-3 independent unknown rel. e displacements. By

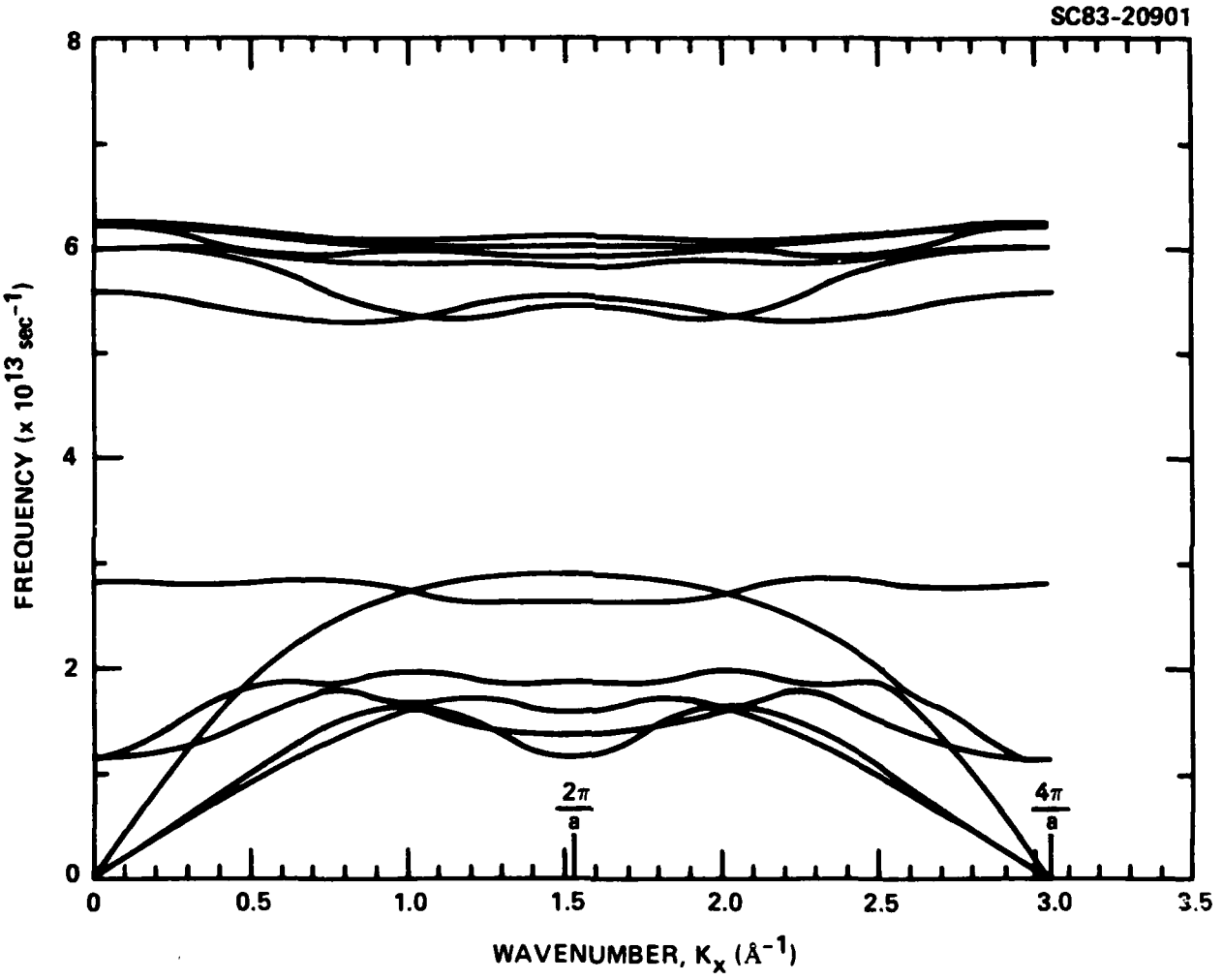

Fig. 4 Lattice dispersion curve for CdS with general (x, y, and z) displacements.

defining these relative displacements to be with respect to the first atom in the unit cell (k=1), Eq. (66) becomes

$$\sum_{k=2}^{N} \sum_{j=1}^{3} \Phi_{m_i,k_j} (\vec{u}_k)_j = e(e_T^*)_{m_i} E_i \qquad (67)$$

where the quantity $[(\vec{u}_k)_j - (\vec{u}_1)_j]$ corresponds to the 3N-3 unknown relative displacements. This above equation is a consequence of

$$\sum_{k=2}^{N} \Phi_{m_i,k_j} = \Phi_{m_i,1_j} \qquad (68)$$

for each combination of m, i and j which can serve as a convenient computation check. Equation (67) still represents a set of 3N linear equations but they are not all independent; for example, the three equations with m=1 can be expressed as a simple linear combination of the remaining 3N-3 equations. The solution to Eq. (67), which will yield the perturbed crystal geometry, can be written analytically in determinant notation as

$$[(\vec{U}_{k'})_{j'} - (U_1)_{j'}] = \det[\Phi_{m_i,k_j} + \{e(e_T^*)_{m_i} E_i - \Phi_{m_i,k_j}\}\delta_{k,k'}\delta_{j,j'}]/\det[\Phi_{m_i,k_j}] \qquad (69)$$

where again $\delta_{k,k'}$ and $\delta_{j,j'}$ are Kronecker delta functions. For N>2, this solution becomes unwieldy and a numerical technique such as the Gauss-Jordan elimination method is more appropriate. The implementation of this numerical procedure is currently in progress using the standard and widely available mathematical subroutine packages. Consequently, results utilizing this

technique are not complete at present and the general application of this method is still speculative.

One final note concerning the lattice response of a crystal to an applied dc electric field is a reminder that the tight-binding formalism for the electro-optic effect (Eq. (41)) depends on the change in the interatomic distance with respect to the applied dc field. This change can be expressed using the notation of Eqs. (41) and (67) as

$$\frac{\partial d_i}{\partial E_k^{dc}} = \frac{[(\vec{u}_m)_i - (\vec{u}_1)_i]}{E_k^{dc}} - \frac{[(\vec{u}_n)_i - (\vec{u}_1)_i]}{E_k^{dc}} = \frac{u_{mni}}{E_k^{dc}} \qquad (70)$$

in the limit of E_k^{dc} approaching zero for $\vec{d}$ being the interatomic distance between atoms m and n.

2.1.5.4 Transverse Effective Charge

The only missing ingredient in the above formalism for the lattice response of a crystal to an applied dc electric field (Eqs. (67) and (70) is the transverse effective charge, $(e_T^*)_{m_i}$. Traditionally, the transverse effective charge has been introduced in order to account for the local polarization induced by relative displacements[1] such as those described above in Eq. (62). Experimentally, there is a splitting of the optical mode frequencies for polar crystals, even at zero wave-vector (K=0). This splitting[14] is a consequence of the added rigidity in longitudinal (but not transverse) lattice modes resulting from the local polarization density induced by the relative displacement of a pair of neighboring atoms with unequal charges. Additionally, this same charge quantifies the coupling between the transverse lattice vibrations and light (i.e., optical electro-magnetic waves) leading to the name: transverse effective charge.

The well-known Lyddane-Sachs-Teller relation can be expressed in terms of a transverse effective charge as follows. Let the optical dielectric constant be

$$\varepsilon_\infty = 1 + 4\pi\chi_e \tag{71}$$

and the static dielectric constant becomes

$$\varepsilon_0 = 1 + 4\pi\chi_e + 4\pi\chi_i = \varepsilon_\infty + 4\pi\chi_i \tag{72}$$

where χ_e is the electronic susceptibility and χ_i is the ionic susceptibility. Now consider two atoms with charges of +q and -q vibrating against each other, with a lattice coupling spring constant, κ. The equation of motion for this system is

$$\kappa(u_2 - u_1) = q(\Delta E) = q(\Delta P)/\chi_i \tag{73}$$

where $(u_2 - u_1)$ is the relative displacement of the two atoms, ΔE is the induced change in the dipole electric field. The induced change in polarization density, ΔP, is

$$\Delta P = \sum_i q_i u_i/\Omega_0 = q(u_2 - u_1)/\Omega_0 \tag{74}$$

where Ω_0 is the volume occupied by the two atoms. Then, the ionic susceptibility becomes

$$\chi_i = q^2/(\Omega_0 \kappa) = q^2/(\Omega_0 \mu \omega_T^2) \tag{75}$$

where $\mu = \kappa/\omega_T^2$ is the reduced mass. Finally, the Lyddane-Sachs-Teller relation[14] is

$$\frac{\omega_L^2}{\omega_T^2} = \frac{\varepsilon_0}{\varepsilon_\infty} = 1 + 4\pi\chi_i/\varepsilon_\infty \tag{76}$$

using Eq. (72). This can be rewritten as

$$\omega_L^2 - \omega_T^2 = 4\pi q^2/(\Omega_0 \mu \varepsilon_\infty) \tag{77}$$

i.e., the difference in the square of the longitudinal and transverse optical mode frequencies is proportional to the effective charge, q, squared.

The concept of transverse effective charge can now be generalized to accommodate a crystal of N atoms per unit cell. The vibrational motion of each atom in the unit cell has been previously described in Eq. (62). However, this equation treats the eigenfrequency of each normal mode without accounting for the change in local polarization density induced by the relative displacements of the atoms. The i-th component of this extra force on the m-th atom in the unit cell is

$$F_{m_i} = \frac{-4\pi}{\Omega_0 \varepsilon_\infty} \sum_{k=1}^{N} e^2 (e_T^*)_{m_i} (e_T^*)_{k_i} [(\vec{u}_k)_i - (\vec{u}_m)_i] \tag{78}$$

and it should be added to the lattice equation of motion (i.e., Eq. (62)). Here, there is an effective transverse charge associated with each normal (lattice vibrational) mode of the crystal. Then, if the approximation that the eigenvectors for the longitudinal optic modes are invariant to this additional perturbation is made, a generalized form of Eq. (77) is obtained:

$$(\omega_L^2 - \omega_T^2)_{m_i} = \frac{4\pi e^2 (e^*_T)_{m_i}}{\Omega_0 \epsilon_\infty M_m} \sum_{k=1}^{N} (e^*_T)_{k_i} (\vec{u}_k)_i / (\vec{u}_m)_i \qquad (79)$$

where M_m is the mass of the m-th atom in the unit cell.

For simple crystal systems, it is possible to use Eq. (79) to infer values for the various transverse effective charges from experimental Lyddane-Sachs-Teller splittings in the optical modes of the lattice vibrational spectrum. However, an approach more aligned with the philosophy of the Bond Orbital Model would be to develop a formalism to predict these transverse effective charges from first principles. The predicted values could then be compared directly to experiment via Eq. (79). In either case, the numerical values for $(e^*_T)_{m_i}$ could then be substituted back into Eq. (67) to give the lattice response of the crystal to an external dc electric field. Finally, this result would permit the numerical evaluation of the ionic contribution to the electro-optic susceptibility (Eq. (41) to be completed.

2.1.6 The Electro-Optic Effect in TeO_2

The chemical bonding in tellurium dioxide can be characterized as a mixed tetrahedral complex in which the tellurium atoms have fourfold coordination while the oxygen atoms have only twofold coordination. In this respect it belongs to the class of materials XO_2, containing compounds such as SiO_2, TiO_2, and Al_2PO_4, which has received considerable attention.[1] In this class of complexes, an atom X is covalently bonded to four oxygen atoms approximately in a tetrahedral configuration. However, in order to describe the

electronic and lattice features of crystals from this class in a simple bond picture, it is more appropriate to choose as a molecular bonding subunit an X-O-X structure comprised of two X hybrid orbitals and the atomic orbitals of an intervening oxygen.[1] Such subunits are analytically coupled so that effects such as susceptibility may be approximately calculated by adding the effects of independent bonding units. It is a generalization of the Bond Orbital Model of tetrahedral semiconductors. This choice of bonding subunit greatly simplifies the calculations in the relatively complex crystal structure of this class of materials, and yields a reasonable estimate of various optical properties like the electric susceptibility. Although the crystal structure of TeO_2 contains a large number of atoms in the unit cell and the detailed structure of the Te-O bonding is in fact more complicated than that in SiO_2, similar aspects of the bonding structure suggest a parallel approach to calculating the susceptibility. Therefore a simplified bond scheme will be applied to TeO_2 in order to calculate a specific second-order susceptibility: the linear dc electro-optic effect.

TeO_2 is an optically anisotropic (positive uniaxial) crystal and is commonly used as an acousto-optic material.[15,16] The linear dc electro-optic coefficient,[17] other nonlinear optical properties,[18-22] and elastic, dielectric and piezoelectric properties,[23] have been experimentally determined. Consequently, a comparison of the Bond Orbital Model prediction for the electro-optic effect will be made with the experimental result.

2.1.6.1 Crystal Structure

Tellurium dioxide has the point group symmetry 422, consistent with the space group $P4_12_12$.[24] The lattice constants are a = 4.796Å and c = 7.626Å, with four tellurium atoms and eight oxygen atoms per unit cell. Each tellurium has four oxygen nearest neighbors. Each oxygen has two tellurium nearest neighbors at different distances 1.92Å and 2.09Å while the Te-O-Te bond angle is 140.8°. The properties considered here vary as the square of the distance and an average of 2.00 Å will be used. The crystallographic unit cell is shown schematically in Fig. 5.

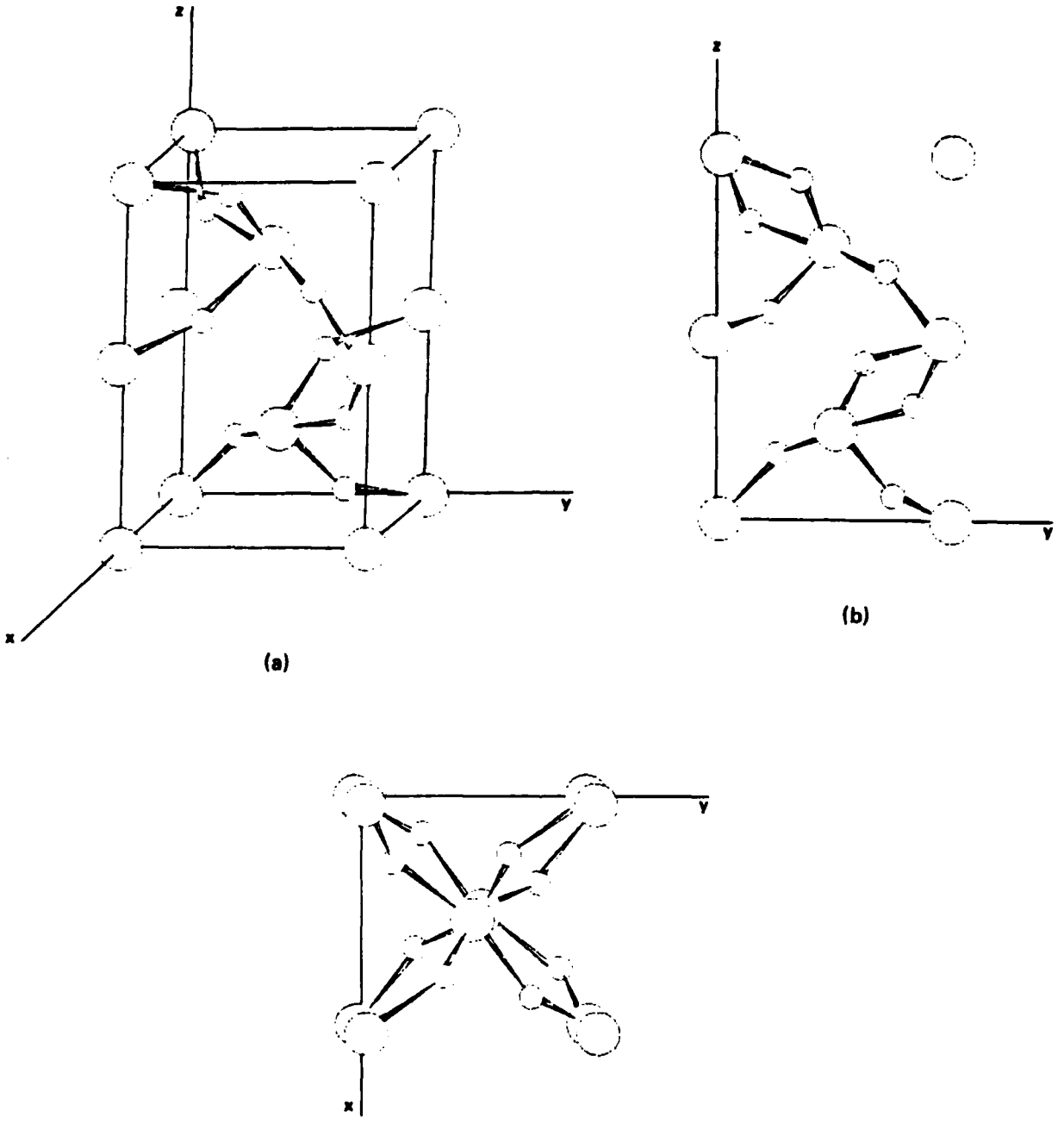

Fig. 5 TeO_2 unit cell with nearest neighbor bonds: (a) 3D perspective, (b) viewed down the x-axis, and (c) viewed down the z-axis.

2.1.6.2 First-Order Susceptibility

Following the Bond Orbital Model formalism presented for SiO_2,[1] the linear susceptibility of TeO_2 can be obtained by calculating the polarizability of each Te-O-Te molecular unit and then summing the eight resulting dipole moments over the unit cell (normalized by the volume of the unit cell).

As an approximation, the electronic structure of a symmetric Te-O-Te subunit may be determined by considering an atomic p-state on each tellurium atom to be spatially directed toward the oxygen atom. This atomic p-state must, in the real system, be some sort of s-p hybridized orbital since each tellurium atom has four nearest neighbor oxygen atoms while only three p-states are available for these four bonds. The two unoccupied tellurium p-states in the Te-O-Te subunit will only significantly interact with the two occupied oxygen p-states in the x-z plane, as illustrated in Fig. 6a. (The oxygen s-state is ignored because its energy is considerably lower than any tellurium state. The s-state on the tellurium is not included since it is occupied and the only unoccupied states are orthogonal tellurium p-states. Lastly, the p_y-state on the oxygen is also orthogonal to these tellurium s-states). To further simplify the calculation, only the ppσ coupling will be included since it is a factor of four larger than the ppπ contribution. Referring to the states identified in Fig. 2a, the bonding (B_x and B_z) and antibonding (A_x and A_z) states for the symmetric Te-O-Te unit in the x and z directions, respectively, are:

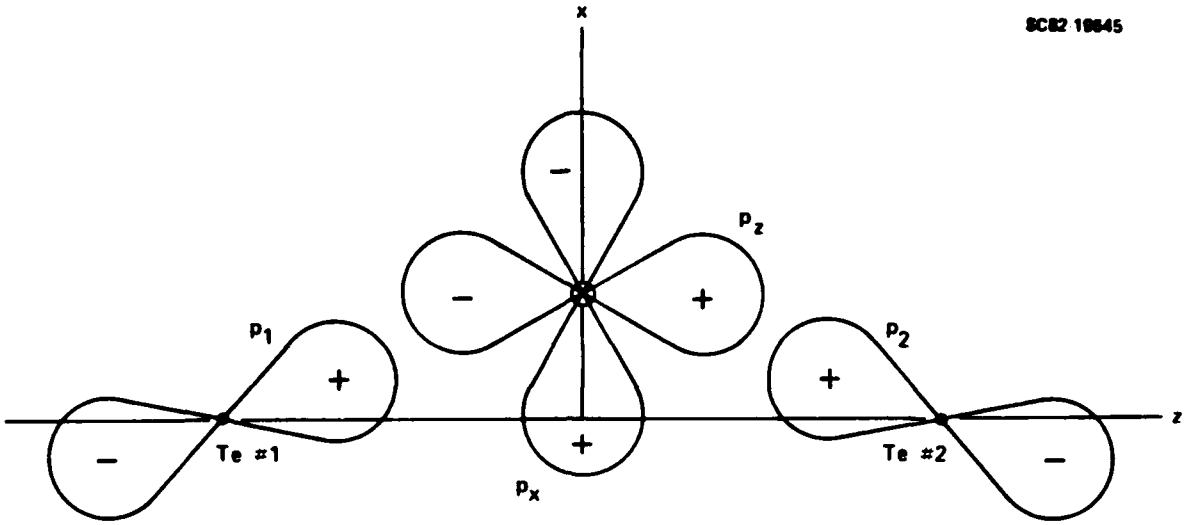

(a)

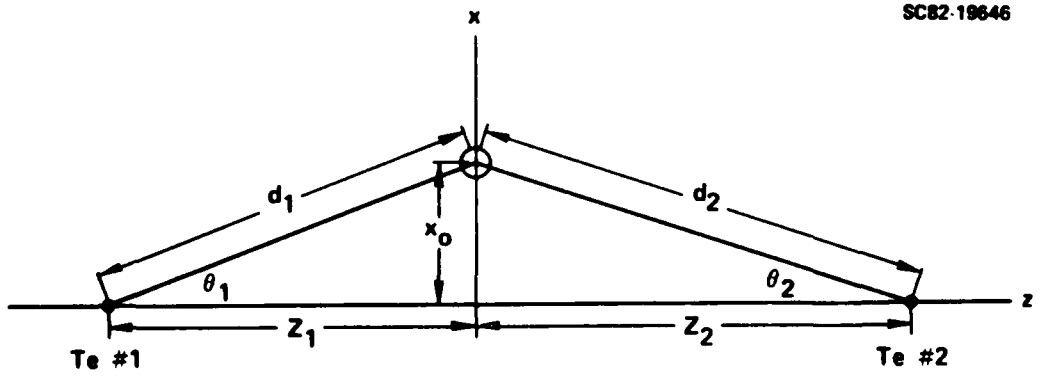

(b)

Fig. 6 TeO_2 molecule subunit: (a) atomic orbital assignments and (b) coordinate system for unsymmetric subunit.

$$B_x = \frac{1}{2}\left[\sqrt{1 - \beta_x}\ (|p_1\rangle + |p_2\rangle) + \sqrt{2 + 2\beta_x}\ |p_x\rangle\right]$$

$$B_z = \frac{1}{2}\left[\sqrt{1 - \beta_z}\ (-|p_1\rangle + |p_2\rangle) + \sqrt{2 + 2\beta_x}\ |p_z\rangle\right] \tag{80}$$

$$A_x = \frac{1}{2}\left[\sqrt{1 + \beta_x}\ (|p_1\rangle + |p_2\rangle) - \sqrt{2 - 2\beta_x}\ |p_x\rangle\right]$$

$$A_z = \frac{1}{2}\left[\sqrt{1 + \beta_z}\ (-|p_1\rangle - |p_2\rangle) + \sqrt{2 - 2\beta_z}\ |p_z\rangle\right]$$

where

$$\beta_x = V_3/\sqrt{V_3^2 + 2V_{pp\sigma}^2 \sin^2\phi}$$

(81)

$$\beta_z = V_3/\sqrt{V_3^2 + 2V_{pp\sigma}^2 \cos^2\phi} \quad .$$

The polar energy for TeO_2 is

$$V_3 = \frac{\varepsilon_p^{Te} - \varepsilon_p^{O}}{2} = 3.59 \text{ eV} \tag{82}$$

while the $V_{pp\sigma}$ plays the role of a covalent energy for the symmetric subunit,

$$V_{pp\sigma} = -2.22 \frac{h^2}{md_I^2} = 4.22 \text{ eV} \tag{83}$$

using the parameters introduced in Ref. (11).

To calculate the polarizabilities of the Te-O-Te subunit, the perturbation of the polar energy, in response to the optical electric field, is considered. This perturbation is $eE_x x$ or $eE_z z$ for the x and z directions, respectively. Writing out the x and z bonding wavefunctions in a first-order perturbation-theory expansion of the antibonding wavefunction gives a polarizability of

$$\alpha_i = \frac{2e^2 \langle B_i | x_i | A_i \rangle^2}{\epsilon_{A_i} - \epsilon_{B_i}} \tag{84}$$

where ϵ_{B_i} and ϵ_{A_i} are the bonding state and antibonding state energies given by

$$\left.\begin{matrix}\epsilon_{B_i} \\ \epsilon_{A_i}\end{matrix}\right\} = \frac{1}{2}(\epsilon_p^{Te} + \epsilon_p^{O}) \left\{\begin{matrix}- \\ +\end{matrix}\right\} V_3/\beta_i \quad . \tag{85}$$

Evaluating the dipole matrix elements in the usual fashion,[1] the polarizabilities become

$$\alpha_x = \frac{e^2 d^2 \sin^2\phi}{2V_3} [\beta_z(1 - \beta_z^2) + \beta_x(1 - \beta_x^2)] \tag{86}$$

$$\alpha_z = \frac{2 e^2 d^2 \cos^2\phi}{V_3} \left[\frac{(1 - \beta_x\beta_z)\, \beta_x\beta_z}{\beta_x + \beta_z}\right] \quad .$$

Numerical evaluation of Eq. (86) for TeO_2 yields

$$\alpha_x = +0.533 \text{ A}^3$$
$$\alpha_z = +5.04 \text{ A}^3 \quad . \tag{87}$$

The first-order susceptibility tensor component, $\chi_{ij}^{(1)}$, is defined by

$$P_i = \sum_j \chi_{ij}^{(1)} E_j \tag{88}$$

where P_i is the induced polarization density and E_j is the optical electric field. We could obtain a susceptibility by averaging the effect of each unit over angle, giving $(\alpha_x + \alpha_z)/3$ (since $\alpha_y = 0$ in our description) and multiply by the density of bonding units $N_o = 8/(a^2c)$ (or oxygen atoms):

$$\chi^{(1)} = N_o (\alpha_x + \alpha_z)/3 = 0.085. \tag{89}$$

As another alternative, the tensor χ_{ij} for the real crystal is determined from the bonding subunit polarizabilities by summing over the eight subunits in the unit cell as follows. The electric field along the j-th crystal coordinate axis must be transformed into an electric field vector in the coordinate system of each Te-O-Te subunit. The x and z components of this transformed electric field induce a dipole moment

$$\vec{p} = \alpha_x E_x \hat{x} + \alpha_z E_z \hat{z} \tag{90}$$

in the Te-O-Te subunit coordinate system. This dipole moment then must be transformed back into the crystal coordinate system. Finally, $\chi_{ij}^{(1)}$ is calculated by summing up the i-th components of the transformed dipole moments from each of the eight Te-O-Te subunits and dividing by the volume of the unit cell. Note that the transformation between the crystal axes and each Te-O-Te subunit coordinate system is different (see Table 1).

In a coordinate system of the crystallographic axes, the calculated linear susceptibilities are

$$\chi_{11}^{(1)} = \chi_{22}^{(1)} = 0.092$$

$$\chi_{33}^{(1)} = 0.071 \quad . \tag{91}$$

Note that these first-order susceptibilities are simply the sum of the individual bond polarizabilities and do not include any corrections due to bond-bond interactions or local field effects. Corrections of this type are sometimes semiempirically taken into account by introdyuing a scaling factor, γ[1] This scaling factor enters in $\chi_{ij}^{(1)}$ as γ^2 and it is used to match the calculated values of $\chi_{ij}^{(1)}$ with those derived from the experimentally measured refractive indices using the relation

$$n_i = \sqrt{1 + 4\pi\chi_{ii}^{(1)}} \quad . \tag{92}$$

Comparison with the experimental values for the ordinary and extraordinary indices, $n_o = 2.26$ and $n_e = 2.41$ respectively,[18] yields an average $\gamma = 2.1$. The significance of this value is that it can now be used for the calculation of the second-order susceptibility without introducing additional scaling

Table 1

The Transformation Between the Crystal Axes and the Te-O-Te Subunit is Specified by the Direction Cosine of Each Crystal Axis With Respect to Each Subunit Axis. The Direction Cosines Are:

	Crystal Coordinates x	y	z		Crystal Coordinates x	y	z		Crystal Coordinates x	y	z		Crystal Coordinates x	y	z
		No. 1				No. 2				No. 3				No. 4	
x	-.695	+.070	+.716	x	+.070	-.695	-.716	x	+.695	+.070	+.716	x	+.070	+.695	+.716
y	+.419	-.769	+.482	y	-.769	+419	-.482	y	+.419	+.769	+.482	y	+.769	+.419	-.482
z	+.584	+.635	+.505	z	+.635	+.584	-.505	z	+.584	-.635	+.505	y	-.635	+.584	-.505
		No. 5				No. 6				No. 7				No. 8	
x	-.070	+.695	-.716	x	-.070	-.695	+.716	x	-.695	-.070	-.716	x	+.695	-.070	+.716
y	+.769	-.419	-.482	y	+.769	+.419	+.482	y	+.419	+.769	-.482	y	-.419	+.769	+.482
z	-.635	-.584	-.505	z	-.635	+.584	+.505	z	+.584	-.635	-.505	z	-.584	-.635	+.505

parameters. It should be pointed out that the calculated sign of the birefringence, $\Delta n = n_e - n_o$, is predicted incorrectly. Within the context of the Bond Orbital Model, the sign of the birefringence is specified strictly by crystal geometry. These differences in the ordinary and extraordinary indices are perhaps be due to the bond-bond coupling or anisotropic local field effects.

2.1.6.3 Second-Order Susceptibility

The second-order susceptibility, $x^{(2)}_{ikj}$, may be divided into two parts: an electronic part and an ionic displacive one. The electronic contributions arise from the changes in the first-order electronic polarizability due to the application of a dc electric field while keeping all atomic positions fixed. Calculations in TeO_2 (point group symmetry 422) show that this electronic contribution vanishes in accordance with the Kleinman's symmetry criterion.[2] The ionic displacive contribution is determined by perturbing the crystal geometry with a dc electric field, as described below, and then recalculating the first-order susceptibility using the formalism given in Section 2.1.6.2. We hold the crystal surfaces rigid or clamped and then do not include any distortion arising from the piezoelectric effect. The second-order susceptibility, and hence the "clamped"[4] electro-optic coefficient, is then proportional to the difference between the two linear susceptibilities associated with the perturbed and unperturbed geometries.

In determining the ionic displacive contribution in the clamped case, the only important degrees of freedom for the electro-optic effect correspond to the IR-active optical modes in which the displacement of an atom gives rise to a net change in the electrical dipole moment. Since the ratio of the Te mass to the O mass is about eight, one can, in principle, decouple the problem of finding the acoustical modes from that of the optical modes. Therefore, only the vibrations of the oxygen atoms in an immobile tellurium lattice will be considered and any coupling between the various local oxygen modes will be neglected. (Note: a detailed description of the vibrational modes in

paratellurite has been given elsewhere.[25]) Thus, again consider a bonding subunit Te-O-Te as in Fig. 6 and now distinguish the two bond lengths which were neglected in the preceding. Letting the elastic motion of the oxygen be characterized by a "bond-stretching" force constant, C_o, which describes the change in Te-O interatomic distance, and a "bond-rocking" force constant, C_1, which describes the tilt of the Te-O-Te unit out of the x-z plane, the elastic energy can be written

$$E = \frac{1}{2} C_o \frac{(d_1' - d_1)^2}{d_1^2} + \frac{1}{2} C_o \frac{(d_2' - d_2)^2}{d_2^2} + \frac{1}{2} C_1 (\delta\xi)^2 \qquad (93)$$

where d'_1 and d'_2 are the time-dependent Te-O bonding distances, d_1 and d_2 are the corresponding equilibrium distances and $\delta\xi$ is the angular tilt. Here, the "bond-bending" force for the Te-O-Te bond angle has been neglected because it is much smaller than the "bond-stretching" force and any oxygen displacement in the x-z plane causes changes in bond length. For the coordinate system shown in Fig. 6b, the equations of motion for the oxygen atom (to first-order in the displacement) are

$$\begin{aligned}
-M\omega^2\Delta x &= -C_o\left[\left(\frac{x_o^2}{d_1^4} + \frac{x_o^2}{d_2^4}\right)\Delta x - \left(\frac{x_o z_1}{d_1^4} + \frac{x_o z_2}{d_2^4}\right)\Delta z\right] \\
-M\omega^2\Delta y &= -\frac{C_1}{x_o^2}\Delta y \qquad (94) \\
-M\omega^2\Delta z &= -C_o\left[-\left(\frac{x_o z_1}{d_1^4} + \frac{x_o z_2}{d_2^4}\right)\Delta x + \left(\frac{z_1^2}{d_1^4} + \frac{z_2^2}{d_2^4}\right)\Delta z\right]
\end{aligned}$$

where z_1 and z_2 specify the tellurium positions and x_o gives the location of the oxygen atom. (Note that the motion in the y-direction is completely

uncoupled from the x and z motions.) In the approximation of a symmetric Te-O-Te unit where $d_1 = d_2$ and $z_1 = z_2$, the three normal vibrational modes are purely along the x, y and z axes with the eigenfrequencies given by

$$\omega_x^2 = \frac{2\, C_o \sin^2\theta}{M\, d_1^2}$$

$$\omega_y^2 = \frac{C_1}{M\, x_o^2} \qquad (95)$$

$$\omega_z^2 = \frac{2\, C_o \cos^2\theta}{M\, d_1^2}$$

respectively, where $\theta = (\pi - \theta')/2$ and θ' is the Te-O-Te bond angle. For the unsymmetric case, the equations of motion can also be obtained in closed form and the resultant set of vibrational modes and frequencies only deviate a small amount from the symmetric case.

The three local mode frequencies ω_x, ω_y and ω_z will be the same for all the oxygen atoms in the unit cell. Allowing for some small frequency distribution for the various oxygen atoms due to coupling between different modes through the tellurium atoms in the real crystal, this local mode approximation leads to three sets (or bands) of optical frequencies, each centered at the local mode frequency given by Eq. (95). Indeed the experimental infrared reflectivity data[26] show distinct bands which can be interpreted as arising from the oxygen local modes. This predicts immediately a ratio $\omega_x/\omega_z = \tan\theta = 0.36$. Assigning the centers of the two highest bands to the frequencies of $\omega_x^{exp't} = 0.70 \times 10^{14}$ sec^{-1} and $\omega_z^{exp't} = 1.45 \times 10^{14}$ sec^{-1} for the bond-stretching local modes and the third one with a frequency of $\omega_y^{exp't} = 0.33 \times 10^{14}$ sec^{-1} for the rocking mode of the Te-O-Te subunit, we find $\omega_x/\omega_z = 0.48$. The following estimates for C_o and C_1 are obtained from Eq. (95):

$$C_0 = 110 \text{ eV}$$

$$C_1 = 8.0 \text{ eV} \qquad (96)$$

where C_0 was determined from the average fit to $\omega_x^{exp't}$ and $\omega_z^{exp't}$. The magnitude of these values for C_0 and C_1 are in reasonable agreement with estimates for bond-stretching and bond-bending force constants in semiconductors.[1] It is worth mentioning here that due to the decoupling of the bond-stretching modes (ω_x and ω_z above) from the Te-O-Te bond-rocking mode (ω_y), the frequency of the latter is determined by C_1 only and is therefore "softer" than the bond-stretching modes. As it turns out, this softer mode makes the major contribution to the electro-optic coefficient since it is most affected by the dc electric field.

In order to estimate the motion of the oxygen atoms in response to an applied dc electric field, we introduce a transverse effective oxygen charge e_T^* associated with each mode.[1] It is defined to be the electric dipole interaction by a single oxygen, divided by the displacement. Expressions to determine these effective charges in terms of the Bond Orbital Model parameters already introduced have previously been derived[1] for the Si-O-Si unit. Using the same expressions for Te-O-Te:

$$(e_T^*)_y = Z^* = \beta_x + \beta_z \qquad (97)$$

$$(e_T^*)_x = Z^* + (3 \sin^2\theta - 1)\, \beta_x(1 - \beta_x^2) + 3 \sin^2\theta\, \beta_z(1 - \beta_z^2)$$

$$(e_T^*)_z = Z^* + (3 \cos^2\theta - 1)\, \beta_z(1 - \beta_z^2) + 3 \cos^2\theta\, \beta_x(1 - \beta_x^2)$$

where β_x and β_z are given in Eq. (81). Numerically evaluating the parameters for a symmetric Te-O-Te subunit gives

$$(e_T^*)_x = 1.40$$

$$(e_T^*)_y = 1.42 \qquad (98)$$

$$(e_T^*)_z = 2.60.$$

Experimentally, these tranverse effective charges give the local polarization induced by the relative oxygen displacements and hence the splitting between the transverse and longitudinal optical modes. For each mode, the transverse effective charge is shown, in Section 2.1.6.5 below, to be given by a Lyddane-Sachs-Teller[14] relation

$$\omega_{LO}^2 - \omega_{TO}^2 = 4\pi(e_T^*)^2 e^2/3m\Omega_o\varepsilon_1 \qquad (99)$$

where e is the electronic charge, M is the mass of the oxygen, Ω_o is the average volume per oxygen atom and $\varepsilon_1 (= \varepsilon_\infty)$ is the optical dielectric constant. Using this relation along with the approximate experimental splittings of $(\omega_{LO}^2 - \omega_{TO}^2) = .093, .028$ and $.326$ sec^{-2} for the x, y and z modes respectively, we obtain experimental transverse effective charges of

$$(e_T^*)_x = 1.75$$

$$(e_T^*)_y = 0.96 \qquad (100)$$

$$(e_T^*)_z = 3.27$$

which can be directly compared with the theoretical estimates given in Eq. (98).

The force, F_i, in the i-th direction on an oxygen atom is given by

$$F_i = e(e_T^*)_i \, E_i^{dc} \qquad (101)$$

where E_i^{dc} is i-th component of the dc electric field in the coordinate system of the Te-O-Te subunit. Finally, substituting this force into Eq. (94) gives the components of the displacements, which can simply be written as

$$\Delta x_i = \frac{-e(e_T^*)_i \, E_i^{dc}}{M \, \omega_i^2} \qquad (102)$$

for the symmetric Te-O-Te subunit. (The displacements for the unsymmetric subunit can also be obtained in an exact (but more complicated) closed form.) These displacements can now be used to generate a perturbed crystal geometry for an appropriate dc electric field and the first-order susceptibility can be recalculated, as in Section 2.1.6.2.

The defining relation for the second-order (electro-optic) susceptibility, $\chi^{(2)}_{ikj}$, is

$$P_i = \sum_j (\chi^{(1)}_{ij} + \sum_k \chi^{(2)}_{ikj} E^{dc}_k) E^{opt}_j \equiv \sum_j \chi^{T}_{ij} E^{opt}_j \qquad (103)$$

where, as before, P_i is the induced polarization density, $\chi^{(1)}_{ij}$ is the first-order susceptibility, E^{opt}_j is the optical electric field, E^{dc}_k is the dc electric field and χ^{T}_{ij} represents the "total" susceptibility. The electro-optic susceptibility tensor is then obtained from the difference:

$$\Delta\chi^{T}_{ij} = \chi^{T}_{ij}(E^{dc}\neq 0) - \chi^{T}_{ij}(E^{dc}=0) = \sum_k \chi^{(2)}_{ikj} E^{dc}_k \qquad (104)$$

where each particular component of the tensor is determined by considering a specific direction for E^{dc}.

The procedure for predicting this electro-optic susceptibility is somewhat similar to that used for the unperturbed linear susceptibility. First, a dc electric field, E^{dc}_k, is applied in the crystal coordinate system of each Te-O-Te subunit and the relative vector displacement of each oxygen, induced by this dc field, is calculated according to Eq. (102). Next, the vector displacement of each oxygen, given in the Te-O-Te subunit coordinate system, must be transformed back into the crystalline axes thus determining the perturbed crystal geometry. The new linear susceptibility can now be calculated and the electro-optic susceptibility obtained from the difference. The process was carried out numerically for fields in each of the three crystal directions for E^{dc}_k. One computational difficulty was encountered involving the magnitude of E^{dc}_k. If E^{dc}_k was too small, then the change in linear susceptibility was less than the computer round-off error in the calculation. On the other hand, if E^{dc}_k was too large, third-order effects

began to appear. Realizing this problem and choosing an appropriate value for the magnitude for E_k^{dc} gave a 3 × 3 × 3 tensor for the electro-optic susceptibility, in which all components are zero except for

$$\chi_{213} = \chi_{312} = -\chi_{123} = -\chi_{321} = 0.37 \times 10^{-7} \frac{cm}{statvolt} \qquad (105)$$

consistent with the symmetry of point group 422. In this numerical evaluation, the result listed in Eq. (105) has been scaled by γ^2 as discussed in Section 2.1.6.2. Finally, the clamped electro-optic coefficient is given by

$$r_{41} = \frac{-4\pi \chi_{213}}{n_e^2 n_o^2} = -0.15 \times 10^{-7} \frac{cm}{statvolt} = -0.51 \times 10^{-12} m/v \qquad (106)$$

where the values for n_e and n_o are theoretical values calculated from Eq. (92) with the linear susceptibility also scaled using the same γ.

An alternative to using the Te-O-Te subunits for calculating the linear and nonlinear susceptibilities is to employ the bond-by-bond approach, as has been typically done with the tetrahedral semiconductors.[11] There, the first-order susceptibility can be written

$$\chi_{ij}^{(1)} = \frac{e^2}{2v} \sum_{bonds} \frac{V_2^2 d_i d_j}{(V_2^2 + V_3^2)^{3/2}} \qquad (107)$$

where e is the electronic charge, γ, V_2 and V_3 are defined in terms of sp^3 hybridization in Ref. 11, d_m is the m-th component of the interatomic distance vector between the bonding atoms, v is the volume of the unit cell and the

summation is over all bonds in the unit cell. Applying this method to the sixteen bonds in the TeO_2 unit cell gives first-order susceptibilities of

$$\begin{aligned} x_{11}^{(1)} &= x_{22}^{(1)} = 0.316 \\ x_{33}^{(1)} &= 0.232 \end{aligned} \tag{108}$$

which can be compared with Eq. (91) after accounting for the use of a slightly different $\gamma = 1.77$ as listed in Ref. 12.

The electro-optic susceptibility and electro-optic coefficient can then be determined within the context of this bond-by-bond method by using Eqs. (103), (104) and (105). The results are

$$x_{213}^{(2)} = x_{312}^{(2)} = - x_{123}^{(2)} = - x_{321}^{(2)} = 0.17 \times 10^{-7} \frac{cm}{statvolt} \tag{109}$$

and

$$r_{41} = - 0.11 \times 10^{-7} \frac{cm}{statvolt} = - 0.37 \times 10^{-12} \frac{m}{v} \tag{110}$$

which compare reasonably well with Eqs. (105) and (106) even though the assumptions about tetrahedral coordinate that went into Eq. (107) are somewhat dubious for TeO_2.

2.1.6.4 Discussion

The relatively close agreement in the results of the molecular Te-O-Te subunit approach and the bond-by-bond approach suggests that the details of the electronic structure may not be as important as the crystal

geometry. This is because the non-zero tensor elements of the susceptibility arise when the components of the dipole moments do not exactly cancel when summed over the unit cell. The extent of the cancellation is strictly a geometrical effect and the results are relatively insensitive to the parameters that represent the electronic structure.

An experimental value for the "unclamped" or constant stress electro-optic coefficient, r_{41}^T, in TeO_2 has previously[17] been determined to be

$$r_{41}^T = - 0.76 \times 10^{-12} \text{ m/V} \quad . \tag{111}$$

The above calculations predicted the "clamped" or constant strain coefficient, r_{41}^S, which can be related to the "unclamped" coefficient by[5]

$$r_{41}^S = r_{41}^T - p_{44}\, d_{14} \tag{112}$$

where p_{44} is a shear photoelastic constant and d_{14} is the piezoelectric constant. The magnitudes of both p_{44} and d_{14} have previously been measured:[15,27] $|p_{44}| = 0.17$ and $|d_{14}| = 0.81 \times 10^{-11}$ C/N .

Substituting in these numbers into Eq. (112) yields two possible experimental values for the "unclamped" electro-optic coefficient, depending on the sign of the product $(p_{44}\, d_{14})$. For $(p_{44}\, d_{14})$ negative,

$$r_{41}^S = + 0.62 \times 10^{-12} \text{ m/V} \tag{113}$$

and for $(p_{44}\, d_{14})$ positive,

$$r_{41}^{S} = - 2.14 \times 10^{-12} \text{ m/V} \quad . \tag{114}$$

This pair of numbers can now be directly compared with Eqs. (106) or (110). If $(p_{44}\ d_{14})$ is less than zero, then the magnitude of the predicted electro-optic coefficient agrees remarkably well with experiment but a discrepancy exists in the sign. The theory determines this sign solely from the crystal geometry. On the other hand, if $(p_{44}\ d_{14})$ is greater than zero, then the sign agrees but the magnitude of the prediction is approximately a factor of four too small. The theory predicts, then, that p_{44} and d_{14} have the same sign.

2.1.6.5 The Lyddane Sachs Teller Relation For TeO_2

The optical vibrational modes for TeO_2 can be rather well separated into three distinct sets, with frequencies ω_x, ω_y, and ω_z. If there were no dipoles associated with them, these oscillators would be treated as identical, with N_0 modes per unit volume, where N_0 is the number of oxygen atoms per unit volume.

To understand the small shifts in frequencies due to electrostatic forces, consider a particular set of oscillators, say those of frequency, ω_z. These are degenerate vibrational modes, one for each oxygen, and could be equivalently written as modes with well-defined wavenumber by giving each local oscillator a displacement amplitude of $\vec{u}e^{i(\vec{k}\cdot\vec{r}_j - \omega_z t)}$, where $\vec{r}_j$ is the atomic position, and this will in fact give the modes which interact with infrared optical fields of a corresponding wavenumber.

As a first problem, assume that every oscillator moves in a direction exactly parallel to the wave-vector, $\vec{k}$, which has been chosen. (This will never be the case, but will make the calculation clear for the interesting case.) If the dipole moment is given by $(e_T^*)_z$ times the displacement of the atom (this is the definition of the transverse charge $(e_T^*)_z$), then the polarization density is $\vec{P} = N_0(e_T^*)_z\ \vec{u}\ e^{i(\vec{k}\cdot\vec{r}_j - \omega t)}$, where $\vec{u}$ is the vector amplitude parallel to $\vec{k}$. The electric field is obtained from the charge

accumulation, $-i\vec{k}\cdot\vec{P}$, through Poisson's Equation. By dividing by the electronic dielectric constant, the net field, and hence the force on each atom given by $e(e_T^*)_z$ times the electric field, is determined and leads to a shift in frequency. This gives the familar Lyddane-Sachs-Teller result for the difference between the longitudinal frequency, ω_{Lz}, and the transverse frequency, ω_{Tz}, (for which there is no charge accumulation and therefore no shift in frequency). It is

$$\omega_{Lz}^2 - \omega_{Tz}^2 = 4\pi(e_T^*)_z^2 e^2 N_0/M\varepsilon_\infty \quad . \tag{115}$$

If we now examine the relevant case for TeO_2 where the orientation of the polarization vector for the ω_z mode is different for each different oxygen, similar charge-polarization-modulated modes result which, without coupling, all have the same frequency. However, in this case, the dipole of each mode makes an angle θ_j with $\vec{k}$ so its contribution to the polarization density is reduced by a factor of cos θ_j. Furthermore, the force felt by the dipole along its direction of motion due to the field of all other dipoles is reduced by cos θ_j so it behaves exactly as if it were aligned with the field but had its effective charge reduced by a factor of cos θ_j. If every dipole had the same θ_j, the Lyddane-Sachs-Teller relation given above would be valid but with $(e_T^*)_z^2$ replaced by $(e_T^*)_z^2 \cos^2\theta_j$. Clearly in our averaged treatment of the local modes, $\cos^2\theta_j$ should be re-laced by its average, one third, for the case of random orientations.

The distinction between longitudinal and transverse modes in this scheme must be clarified. The phase for each local mode was chosen so that the sign of the polarization along $\vec{k}$ was the same for neighboring atoms, corresponding to a longitudinal mode. Had a particular transverse direction been selected and the sign in that direction chosen to be the same for neighboring atoms, a mode with transverse polarization would have been obtained but the longitudinal components would have cancelled on average, and there would

have been no shift in frequency. Clearly, at long wavelengths, there are longitudinal and transverse optical modes just as there are longitudinal and transverse acoustic modes. There is no difficulty for the long wavelengths of interest here and the relation for our system becomes

$$\omega_{Lz}^2 - \omega_{Tz}^2 = (e_T^*)_z^2 \; e^2 N_0/(3M\epsilon_\infty) \quad . \tag{116}$$

The corresponding expressions, with the same factor of one third, may be written for the x- and y-modes.

2.2 Experimental

2.2.1 *The Electro-Optic Effect in Tl_3AsSe_3*

We have completed measurements of the linear electro-optic tensor component ($r_c = +1.5 \times 10^{12}$m/V) for the chalcogenide salt Tl_3AsSe_3 (TAS). TAS crystallizes[28] the trigonal space group R3m, with the point group 3m. This implies the electro-optic tensor has the following form:[4]

$$r_{ij} = \begin{pmatrix} r_{11} & 0 & r_{13} \\ -r_{11} & 0 & r_{13} \\ 0 & 0 & r_{33} \\ 0 & r_{51} & 0 \\ r_{51} & 0 & 0 \\ 0 & -r_{11} & 0 \end{pmatrix} \tag{117}$$

The dc electric field was applied along the crystallographnic z axis. With

the light propagating along $\underline{x}$, polarized 45° from $\underline{z}$ towards $\underline{y}$, and the dc field applied along $\underline{z}$, the dielectric impermeability tensor[4] has the form

$$B_{ij} = \begin{pmatrix} \frac{1}{n_o^2} & 0 & 0 \\ 0 & \frac{1}{n_o^2} + r_{13}E_3 & 0 \\ 0 & 0 & \frac{1}{n_e^2} + r_{33}E_3 \end{pmatrix} \tag{118}$$

Multiplying by the appropriate polarization tensors, we find:

$$\hat{p}\tilde{B}\hat{p} = \frac{1}{\sqrt{2}}(0\ 1\ 1) \begin{pmatrix} \frac{1}{n_o^2} & 0 & 0 \\ 0 & \frac{1}{n_o^2} + r_{13}E_3 & \\ 0 & 0 & \frac{1}{n_e^2} + r_{33}E_3 \end{pmatrix} \frac{1}{\sqrt{2}} \begin{pmatrix} 0 \\ 1 \\ 1 \end{pmatrix}$$

$$= \frac{1}{2}\left(\frac{1}{n_o^2} + r_{13}E_3 + \frac{1}{n_e^2} + r_{33}E_3\right)$$

$$= B_o + \Delta B \tag{119}$$

which implies that

$$\Delta B = \frac{1}{2}(r_{13} + r_{33})E_3 \quad . \tag{120}$$

For this propagation direction, the effective index is:

$$n_e = \frac{2n_e n_o}{\sqrt{2(n_o^2 + n_e^2)}} \quad . \tag{121}$$

If we assume the incident wave is linearly polarized at 45° to the optical axis upon entry into the crystal, the propagating wave can be decomposed into the two orthogonal modes (ordinary and extraordinary) in the crystal. As the wave travels through the crystal, these two modes get out of phase with one another due to their different propagation velocities. The accumulated phase difference Γ at the exit surface of the crystal is given by:

$$\Gamma = \frac{2\pi\ell}{\lambda_o}(n_e - n_o) \tag{122}$$

where ℓ = the crystal length and λ_o = the free-space wavelength. Thus the emerging beam will, in general, be elliptically polarized due to the arbitrary phase between the energy in each of the two modes. Experimentally, we may quantify the ellipticity through the use of a Babinet Compensator and a final linear polarizer analyser. The application of a transverse dc electric field may affect this propagating beam in three ways. First because TAS is also piezoelectric, the electric field may change the physical dimensions of the sample due to electrically induced mechanical strain:

$$\varepsilon_j = d_{ij} E_i \quad . \tag{123}$$

In this case $E_i = E_3$ so we have

$$\begin{aligned} \varepsilon_1 &= d_{31} E_3 \\ \varepsilon_2 &= d_{31} E_3 \\ \varepsilon_3 &= d_{33} E_3 \end{aligned} \tag{124}$$

The two strain components ε_2 and ε_3 do not produce a direct mechanical effect on the sample which effects our measurement. However ε_1 which is a contraction (or expansion) of the crystal along $\underline{x}$, will change the physical length of the sample. This in turn will produce a change in the phase at the exit surface. Although no direct experimental measurement of the piezoelectric effect in TAS exists, we can assume that it is small consistent with similar semiconducting materials like GaAs. Thus the <u>direct</u> mechanical perturbation will be ignored and the measurement will provide only the "unclamped" value for the electro-optic coefficient. There is, however, a second-order <u>indirect</u> effect often referred to as the converse piezo-optic effect in which the electrically induced strain couples to the refractive index via the strain-optic effect. The strain-optic effect produces on index change:

$$\Delta n_i = -\frac{n^3}{2} p_{ij} \varepsilon_j \tag{125}$$

where p_{ij} is the strain-optic coefficient and ε_j is the strain component as before. Then

$$\Delta n_i = -\frac{n^3}{2} p_{ij} d_{kj} E_k \tag{126}$$

or we may define an effective converse-piezoelectric electro-optic tensor component:

$$r_{ik}^{eff} = p_{ij} d_{kj} \quad . \tag{127}$$

The photo-elastic tensor for the point group 3m is given by:

$$p_{ij} = \begin{pmatrix} p_{11} & p_{12} & p_{13} & p_{14} & 0 & 0 \\ p_{12} & p_{11} & p_{13} & -p_{14} & 0 & 0 \\ p_{31} & p_{31} & p_{33} & 0 & 0 & 0 \\ p_{41} & -p_{41} & 0 & p_{41} & 0 & 0 \\ 0 & 0 & 0 & 0 & p_{44} & p_{41} \\ 0 & 0 & 0 & 0 & p_{14} & 1/2\,(p_{11} - p_{12}) \end{pmatrix} \tag{128}$$

Again taking $E_k = E_3$, and noting the non-zero elements of both the p_{ij} tensor and the d_{kj} tensor, we find the remaining non-zero components are:

$$\begin{aligned} (\Delta n)_1 &= -\frac{n_1^3}{2} (p_{11} d_{31} + p_{12} d_{32} + p_{13} d_{33}) E_3 \\ &= -\frac{n_1^3}{2} [(p_{11} + p_{12}) d_{31} + p_{13} d_{33}] E_3 \end{aligned} \tag{129}$$

$$(\Delta n)_2 = -\frac{n_2^3}{2}(p_{21}d_{31} + p_{22}d_{32} + p_{23}d_{33})E_3$$

$$= -\frac{n_2^3}{2}((p_{12} + p_{22})d_{31} + p_{13}d_{33})E_3$$

$$(\Delta n)_3 = -\frac{n_3^3}{2}(p_{31}d_{31} + p_{32}d_{32} + p_{33}d_{33})E_3$$

$$= -\frac{n_3^3}{2}(2(p_{31}d_{31}) + p_{33}d_{33})E_3 \quad . \qquad (130)$$

Thus we note that both the y and z components of the index (ordinary and extraordinary respectively) will be affected by the dc elecric field. At present, data for the magnitude of p_{11} and p_{33} have been taken at this laboratory under company sponsored IR&D program, but no data exists for the remaining photoelastic components or the piezoelectric tensor components. Thus although, as shown below, we were able to measure a value for the "electro-optic" effect, it is at present not possible to quantitatively separate out effect due to the piezoelectric effect and the converse piezo-optic effect.

2.2.2 Measurement of the Electro-Opic Effect in TAS

A single crystal boule of TAS was grown from the melt using the vertical Bridgman-Stockbarger technique.[29] An experimental sample of dimensions 1.27 cm × 0.54 cm × 0.56 cm was wire sawed from the boule, aligned using back reflection Laue photographs, and mechanically polished. The sample geometry is as shown in Fig. 7. In our early experiments a wire grid polarizer was used as an analyzer after the crystal. A compensator was placed between the sample and the analyzer. The compensator and analyzer were then adjusted so that essentially no light was transmitted through the analyzer to the

SC81-13290

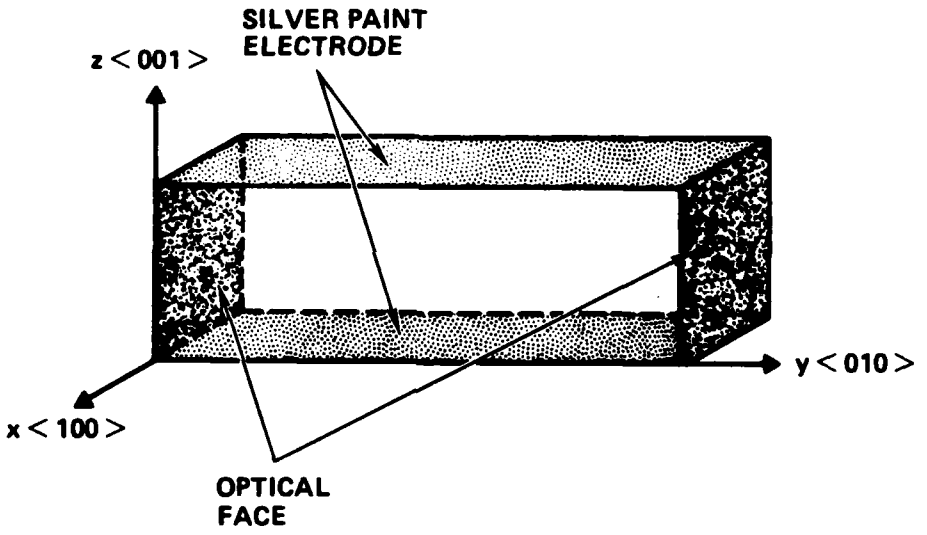

Fig. 7 Tl_3AsSe_3 crystal orientation for r_c electro-optic measurement.

detector. As the dc electric field was slowly increased, a series of oscillations in the signal level at the detector was observed (see Fig. 8). However, further experiments showed that these preliminary results were the result of joule heating of the sample due to an excessive current flowing through the sample when high voltage was applied. Indeed it was possible to reproduce the oscillating transmission by blowing hot air from an electric heat gun across the sample with no applied dc voltage. This excessive current was produced by a low value for the bulk resistivity in the sample. Rather than pursue the traditional methods to remove impurities and defects to obtain intrinsic resistance, which tend to be extremely costly and time consuming, we have chosen an altrnative approach. A high voltage pulser,[27] shown in Fig. 9, was used to apply pulses of high voltage to the sample. The pulse width was kept short and the repetition rate correspondingly low so that the duty cycle was reduced and consequently heating effects were reduced if not eliminated. The average power dissipated in the sample was typically of the order of 1 mW. A high-speed (150 MHz) current-to-voltage amplifier was used in conjunction with a small area InSb photodiode to observe the change in optical transmission produced by the applied high voltage pulse. It should be pointed out, however, as shown in Fig. 10, the pulse was sufficiently long as to allow time for mechanical response of the sample. That is to say, the measurement was made under constant stress conditions (unclamped). The signal from the amplifier was then fed to one channel of an oscilloscope and displayed simultaneously with the high voltage pulse. The process of taking data consisted of (1) setting the amplitude of the high voltage pulse, (2) reading the amplitude of the optical signal as a function of analyzer angle (over 90° of rotation) and (3) then repeating this process at several peak pulse voltages. One can show that for propagation of light polarized at an angle, α, relative to the optical axis, through a birefringent medium and through an analyzing polarizer oriented at an angle, θ, (relative to the optical axis), the resulting transmission will be:

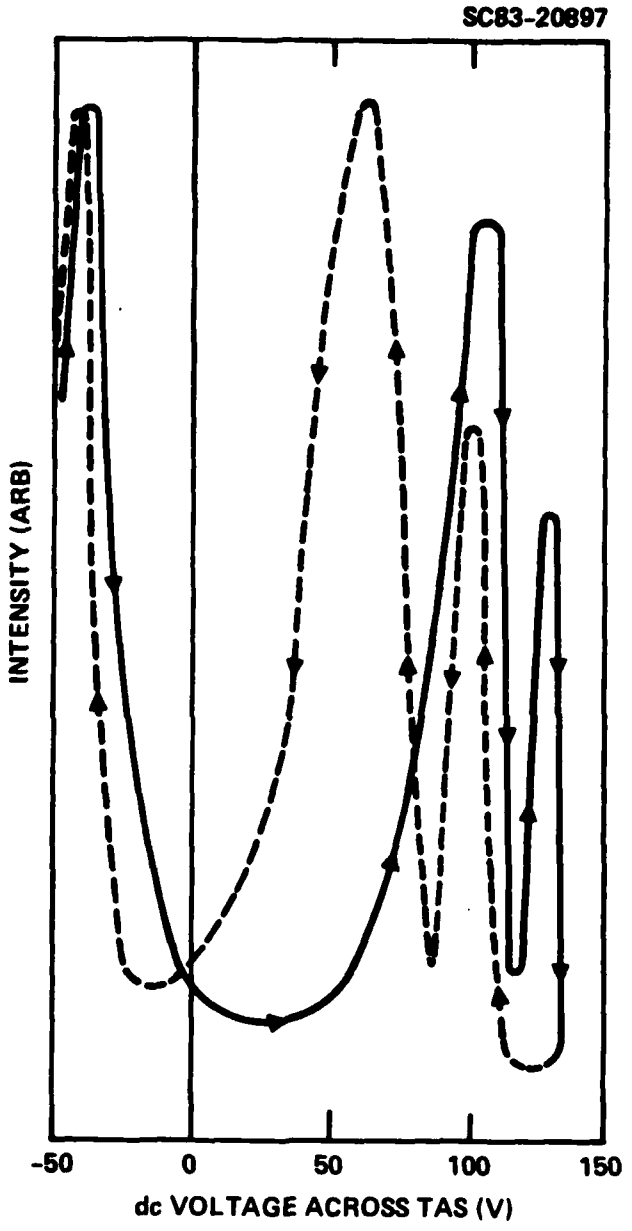

Fig. 8 Intensity modulation as a function of applied dc electric field in Tl_3AsSe_3.

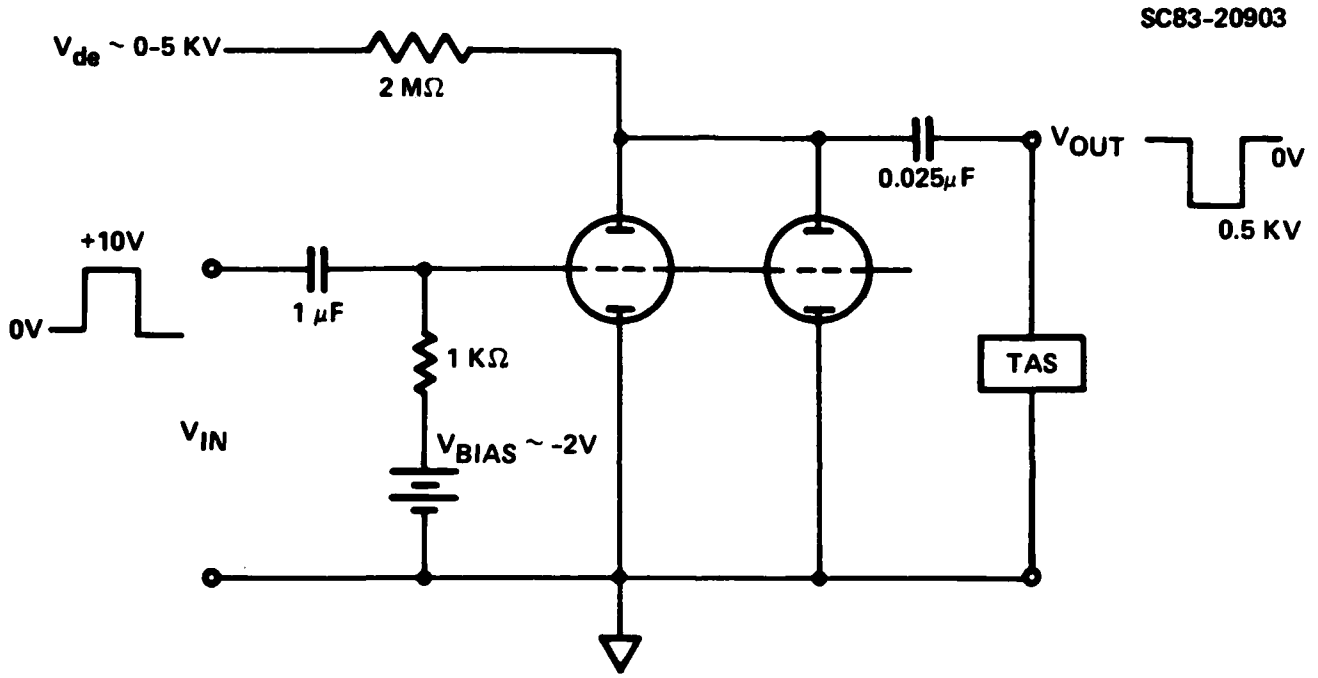

Fig. 9 Circuit diagram for high voltage pulser.

SC83-20904

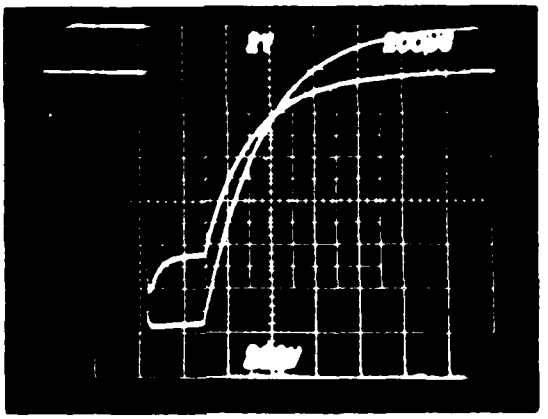

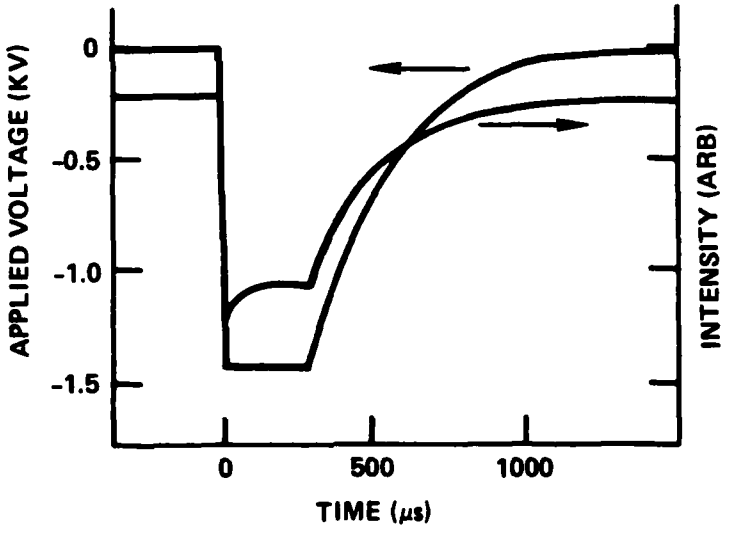

Fig. 10 High voltage pulses applied to Tl_3AsSe_3 and resulting modulation of analyzed light intensity transmitted through Tl_3AsSe_3.

$$I(\theta,\alpha) = \frac{1}{2} I_o \sin^2\alpha\sin^2\theta + \cos^2\alpha\cos^2\theta + 2\sin\alpha\cos\theta\sin\theta\cos\left(\frac{2\pi\ell\Delta n}{\lambda}\right) \quad . \tag{131}$$

If the propagating medium is an electro-optic material oriented similar to our sample, then an applied dc electric field will modify the term containing Δn via the electro-optic effect. The difference in intensities with the electric field on and off is

$$\Delta I(\theta,\alpha,E) = I_0 \sin\alpha\cos\alpha\sin\theta\cos\theta \left\{\cos\left[\frac{2\pi\ell}{\lambda}\left(\Delta n + \frac{n_0^3}{2} r_c^{eff} E\right)\right] - \cos\left(\frac{2\pi\ell}{\lambda}\Delta n\right)\right\} \quad . \tag{132}$$

This change in transmitted intensity as a function of analyzer angle, θ, for a given "dc" electric field is precisely the data we have obtained experimentally. The data can then be numerically fitted to the above expression to yield a value for r_c^{eff}. Figure 11 shows a fit to the experimental data. This process yields a value of $r_c^{eff} \approx +1.5 \times 10^{12}$ m/V at T = 300K and λ = 3.39 μm. As previously indicated, more data is needed to explicitly solve for each of the various contributions to this value. Future studies on TAS hopefully will supply this information.

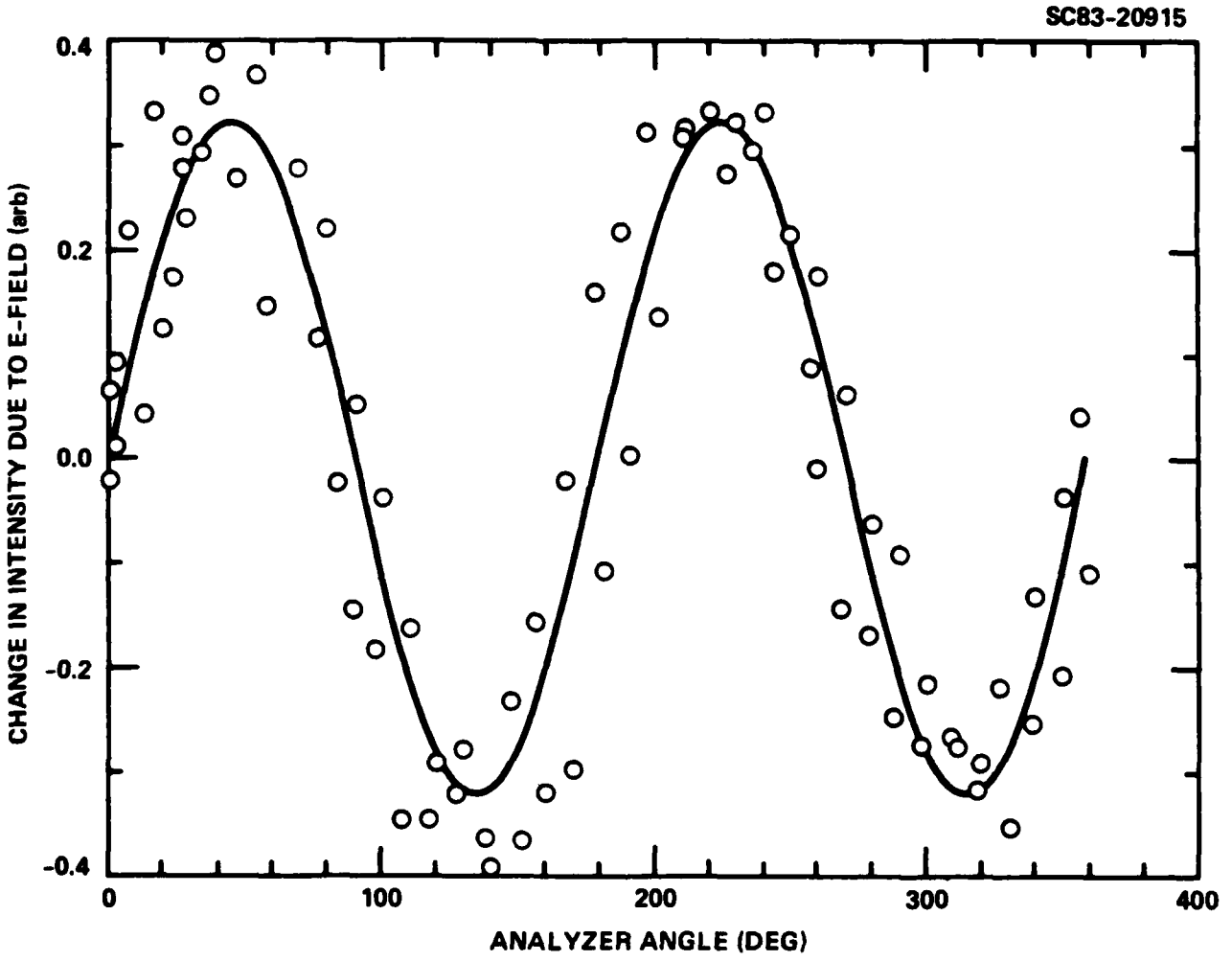

Fig. 11 Intensity difference between "dc" field applied and zero field as a function of analyzing polarizer angle.

3.0 CONCLUSION

In summary, the microscopic understanding of the electro-optic effect has progressed substantially during the course of this program. A tight-binding theory for dielectric susceptibilities has been specifically applied to the linear dc (Pockel's) effect. The distinction between electronic and ionic contributions was explicitly maintained. A formalism to address the generalized lattice dynamic problem, associated with the ionic contribution to the electro-optic effect, has been developed using a method which should be applicable to all materials, e.g., ferroelectric crystals that exhibit large electro-optic coefficients.

4.0 REFERENCES

1. W.A. Harrison, Electronic Structure and the Properties of Solids, (Freeman, San Francisco, 1980).

2. D.A. Kleinman, Phys. Rev. 126, 1977 (1962).

3. M.D. Ewbank and P.R. Newman, J. Appl. Phys. 53, 1150, (1982).

4. I.P. Kaminow and E.H. Turner, in Handbook of Lasers, ed. by R.J. Pressley (Chemical Rubber Co., Cleveland, p. 447, 1971).

5. J.F. Nye, Physical Properties of Crystals, (Univ. Press Oxford, Eng., 1976) p. 124.

6. D.F. Nelson, J. Opt. Soc. Am. 65, 1144 (1975).

7. G.D. Boyd and D.A. Kleinman, J. Appl. Phys. 39, 3597 (1968).

8. P.A. Franken and J.F. Ward, Rev. Mod. Phys. 35, 23 (1963).

9. M. Bass, P.A. Franken and J.F. Ward, Phys. Rev. 138, A534 (1965).

10. A. Yariv, Quantum Electronics, (J. Wiley and Sons, Inc. N.Y., 1975).

11. W.A. Harrison, Phys. Rev. B24, 5835 (1981).

12. L.I. Schiff, Quantum Mechanics (McGraw-Hill, N.Y., 3rd ed., 1968) p. 404.

13. W.A. Harrison, "Elementary Quantitative Theory of Chemical Bonding," in Structure and Bonding in Crystals, Vol. I (Academic Press, Inc., N.Y., 1981) pp. 137-154.

14. R.H. Lyddane, R.G. Sachs and E. Teller, Phys. Rev. 59, 673 (1941).

15. N. Uchida and Y. Ohmachi, J. Appl. Phys. 40, 4692 (1969).

16. T. Yano and A. Watanabe, J. Appl. Phys. 45, 1243 (1974).

17. M. D. Ewbank and P. R. Newman, J. Appl. Phys. 53, 1150 (1982).

18. S. Singh, W. A. Bonner and L. G. Van Vitert, Phys. Lett. 38A, 407 (1972).

19. D. S. Chelma and J. Jerphagnon, Appl. Phys. Lett. 20, 222 (1972).

20. L. M. Belyaev, A. V. Gil'vars, ⁝. M. Dorozhkin, V. A. Kizel', V. M. Koval'chuk and S. P. Smirnov, JETP Lett. 17, 142 (1973).

21. B. F. Levine, IEEE J. Quan. Elec. QE-9, 946 (1973).

22. M. Okada, K. Takizawa, and S. Ieiri, J. Appl. Phys. 48, 4163, (1977).

23. Y. Ohmachi and N. Uchida, J. Appl. Phys. 41, 2307 (1970).

24. J. Leciejewicz, Z. Kristallog, 116, 345 (1961).

25. V. Lemos, F. Cerdeira and M. Cardona, Phys. Stat. Sol. b88, 199 (1981).

26. D. M. Korn, A. S. Pine, G. Dresselhaus and T. B. Reed, Phys. Rev. B8, 768 (1973).

27. Y. Ohmachi and N. Uchida, J. Appl. Phys. 41, 2307 (1970).

28. H. Y-P Hong, J.C. Mikkelsen and G.W. Roland, Mat. Res. Bull. 9, 365 (1974).

29. H. Kuwamoto, "Seeded Growth of Tl_3AsSe_3," submitted to Mat. Res. Bull.